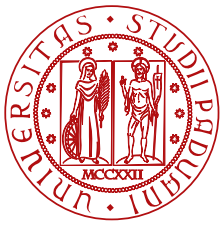

UNIVERSITÀ DEGLI STUDI DI PADOVA

DIPARTIMENTO DI INGEGNERIA DELL'INFORMAZIONE

DEPARTMENT OF INFORMATION ENGINEERING

MASTER DEGREE IN INDUSTRIAL BIOENGINEERING

Degradable hydrogels with simultaneous presence of boron compounds and cell adhesion domains for the muscular reconstruction

Supervisor
Prof. Brusatin Giovanna

Graduating student
Ferrara Martina

Co-supervisors
Prof. Gallego Ferrer Gloria
Dr. Rico Tortosa Patricia María
Dr. Gonzalez Valdivieso Juan

ACADEMIC YEAR 2023-2024

Graduating date 09/07/2024

Sometimes, when you are in a dark place, you think you have been buried.
But actually, you have been planted.
- Christine Caine

Contents

Abstract **9**

Sommario **11**

1 Introduction **13**

1.1 Overview . . . 13

1.2 Aim and goals of the project . . . 14

2 State of the art **15**

2.1 The muscular tissue and its pathologies . . . 15

2.2 The ECM, its components and interactions . . . 18

2.2.1 ECM . . . 18

2.2.2 Fibronectin . . . 19

2.2.3 RGD sequence . . . 20

2.2.4 Integrins . . . 21

2.3 Tissue engineering and existing solutions . . . 22

2.4 Biomaterials . . . 23

2.4.1 Naturally derived materials . . . 25

2.4.2 Hydrogels . . . 28

2.4.3 Synthetic materials . . . 30

2.4.4 PEG Hydrogels and crosslinkers . . . 31

2.4.5 PEG Hydrogels applications . . . 33

2.5 Boron and its current applications . . . 36

3 Materials and methods **41**

3.1 Physico-chemical characterization of the PEG-Hydrogels . . . 41

3.1.1 Synthesis . . . 41

3.1.2 Swelling . . . 44

3.1.3 Degradation . . . 44

3.1.4 Rheology . . . 45

3.2 In vitro assays . . . 46

3.2.1 Cell culture . . . 46

3.2.2 MTS assay . . . 47

3.3 CAM assay 51
3.3.1 Statistical analysis 54

4 Results and discussion **55**
4.1 Physico-chemical characterization of the PEG-Hydrogels 55
4.1.1 Swelling 56
4.1.2 Degradation 58
4.2 Rheology 60
4.3 In vitro assay 64
4.3.1 MTS assay 64
4.4 CAM assay 66

Bibliography **75**

List of Figures

1.1 Centro de Biomateriales e Ingeniería Tisular (CBIT) at the Universitat politècnica de València (UPV). 13

1.2 From left to right: Rodriguez Romano, myself (Martina Ferrara), and Dr Gonzalez Valdivieso at the CBIT 13

2.1 Representation from [2] of the skeletal muscle made of myofibers: each one is surrounded by basal lamina, contains arrays of myofibrils and includes actin and myosin microfilaments. 15

2.2 A schematic portrayal from [2] of a skeletal muscle fiber which depicts a mature muscle fiber as a cluster of myofibrils enveloped by the sarcolemma. 15

2.3 A schematic depiction from [3] of the sarcomere in striated skeletal muscle which illustrates the layout of thick and thin filaments, while also pinpointing the regions of overlap between them. 16

2.4 Schematic representation from [6] of the composition and structure of ECMs loose connective tissue (A), and specialized connective tissues such as cartilage (B), bone (C) and cornea (D) 18

2.5 Schematic representation from [8] of the composition and the principal domains of the fibronectin 19

2.6 Schematic representation of the chemical composition of the RGD sequence from [9] 20

2.7 A model from [9] for the recognition of the fibronectin RGD site and auxiliary sites by an integrin. 21

2.8 Chemical structure of the creatine from [13] usually assumed by athletes in the form of powder to be diluted. 22

2.9 Representation from [31] of the structure of a fiber of Collagen 25

2.10 Representation of the chemical structure of HA from [36] 26

2.11 Formulas of a) PEO b) PEG c) PVA from [53] 29

2.12 PEG chemical structure from [60] 32

3.1 Utilized liquid mixture for the hydrogels before their crosslinking 41

3.2 AX205 DeltaRange - Mettler Toledo balance for the weights measurements 41

3.3 Hydrogels utilized in the following experiments: three per condition. 42

3.4 Utilized weights for the synthesis of the different hydrogels (three for each condition) . . . 43
3.5 Utilized volumes of PBS+/+ for dilution (above) and to put in each well for the construction of the different samples (three each) . . . 43
3.6 Equation 1: Calculation of the swelling percentage rate where wf is the final weigh, while w0 is the initial one . . . 44
3.7 Equation 2: Calculation of the degradation percentage rate where w0 is the initial weight and wf is the final one. . . . 44
3.8 Discovery HR-2 hybrid rheometer during the test . . . 45
3.9 Zoom of the same test from the previous image . . . 45
3.10 Tube containing wild type cells (WT) and normal medium after the centrifuge 47
3.11 Nikon DS-Fi1 Microscope . . . 48
3.12 MTS samples before the analysis with the spectrophotometer (above: the live and death control for the two cell lines, below: the four conditions for the experiment. . . . 49
3.13 PERKIN ELMER Victor X3 Multilabel Reader Board Spectrophotometer 50
3.14 Cut of the air chamber through a milling cutter and the help of a pair of tweezers. . . . 52
3.15 Leica MZ APO X16 magnification microscope utilized for the verification of angiogenesis in the embryos. . . . 52
3.16 ImageJ software . . . 52
3.17 Highlighted blood vessels with the Image J software . . . 53
3.18 AngioTool software utilized to highlight the characteristics of the vessels and obtain the data . . . 53

4.1 Table above: the obtained data of the three samples for each type, after the weigh. Table below: the calculated average of the % of swelling for each type of sample. . . . 56
4.2 On the left: the general trend of the samples when immerged in MilliQ water after different time periods. On the right: a zoom of the first figure representing the analysis and its results from 0 to 60 minutes. . . . 57
4.3 Table above: the obtained data of the three samples for each type, after the weigh. Table below: the calculated average of the % of degradation for each type of sample. . . . 58
4.4 On the left: the general trend of the samples at different time periods in collagenase. On the right: a zoom of the first figure which highlights the trend between 0 and 8 hours. . . . 59
4.5 Graphics of the tangent delta and the complex modulus obtained with the Strain sweep analysis . . . 60
4.6 Graphics of the Storage modulus in function of frequency and time obtained with the Frequency sweep analysis . . . 60

4.7 Graphics of the Loss modulus in function of frequency and time obtained with the Frequency sweep analysis . . . 61
4.8 Graphics of the tangent delta and the complex viscosity obtained with the Frequency sweep analysis . . . 61
4.9 Storage and Loss modulus obtained from the tests of the different samples 61
4.10 Tangent delta (tan δ) consequently calculated by the ratio of Loss and Storage modules . . . 62
4.11 Equation 3: Formula in which E is the Young modulus, G' is the Storage modulus and ν is the Poisson modulus which, for hydrogels, is 0.5 . . . 63
4.12 Equation 4: Results of the Young modulus for each condition (CTRLS, PEG-RGD, PEG-RGD-B and PEG-RGD-BTZ . . . 63
4.13 Cells photos of the 24h MTS assay . . . 64
4.14 Cells photos of the 72h MTS assay . . . 64
4.15 Results of the MTS assay at 24 hours . . . 65
4.16 Results of the MTS assay at 72 hours . . . 65
4.17 Photos taken of the Ferraravascularisation of the CAM for every condition 67
4.18 corresponding masks for the photos taken and reported on the left . . . 67
4.19 Representation of Lacunarity, Branching Index, Number of end points, Number of junctions, Vessels density, Total vessels length and Average vessels length obtained with Graph pad software, where the p value corresponds to: $* \leq 0.05; ** \leq 0.01; *** \leq 0.001; **** \leq 0.0001$. . . . 69

Acknowledgements

First of all, I would like to thank my Italian supervisor, Professor Brusatin, for always supporting me on this path, believing in me and leading me towards a course that made me fall in love with the field of research and engineering, somehow making me find my 'place in the world'.
Secondly, I would like to say thank you to my supervisors from Spain, Dr. Rico Tortosa and Dr. Gonzalez, for always making me feel at home, even when the work was hard, and for always supporting me in the best way possible.
I would also like to thank my family, in particular my parents and my brother Marco, who, besides having allowed me to live these wonderful life experiences, have taught me values that I believe in and I will carry in my heart until the end, both at work and outside. Thank you for all the love and support you constantly showed me, accompanying me in my choices.
I would also like to thank all my close friends whom I have had the pleasure of meeting during my life, in the academic field and beyond. They have been my strength and I will always remember the good times we had together.
Thanks also to Inma and Teresa who, in Spain, were my guardian angels in every situation. I hope this friendship will last forever.
I would also like to thank Federico, the person who has always been there for me, who has given me strength and has never stopped being by my side in any situation. Thank you for believing in me even more than I do.
Finally, I would like to thank myself, for working hard and never giving up, for facing every situation, even difficult ones, always with a smile on her face.
YOU did this.

Abstract

Muscular injuries, whether from trauma, ageing, or pathological conditions like dystrophies, often require invasive interventions or transplants and sometimes lack effective solutions, as seen in Duchenne or Becker dystrophies.
Tissue engineering offers a promising, biocompatible alternative. This master thesis explores the development of PEG (polyethylene glycol) hydrogels composed of PEG-4MAL and two crosslinkers, VPM and PEG-diSH, used in 50:50 ratio. Therefore, the hydrogels containing the VPM peptide, degradable by metalloprotease MMPs, combined with PEG-diSH, result in a controlled degradation rate of the hydrogels of the 50%.
These 3D structures were further enriched with RGD (a cell adhesion motif) and boron compounds such as Bortezomib, aiming to activate NaBC1 boron transporter and the binding-integrins present on the surface of cells. This activation fosters cellular adhesion, proliferation, and differentiation.
This master thesis project mainly focused on the analysis of the material's physicochemical properties and its biocompatibility.
The study involved several experimental setups: pure PEG, PEG-RGD, PEG-RGD-Boron and PEG-RGD-Bortezomib.
Swelling assays were performed to measure water absorption capacity and physical stabilization over time. Degradation assays were carried out to evaluate the enzymatic degradation of the hydrogels (due to the VPM).
Rheological tests using a hybrid rheometer assessed the visco-elastic properties through strain and frequency sweeps.
Biocompatibility was then verified in vitro using an MTS assay with two human fibroblast lines, measuring cell viability and toxicity of the material itself.
Additionally, in vivo tests were conducted using fertilized eggs, evaluating vascularization by analyzing angiogenesis.
This work takes part of a bigger research project which has the main aim to study muscular regeneration. Further experiments could involve the verification of the actual cell adhesion, proliferation and differentiation.
This tissue engineering field holds significant promise for muscular regeneration, potentially offering solutions for currently untreatable conditions.

Sommario

Le lesioni muscolari, siano esse dovute a traumi, invecchiamento o condizioni patologiche come le distrofie, spesso richiedono interventi invasivi o trapianti e talvolta mancano di soluzioni efficaci, come si osserva nelle distrofie di Duchenne o Becker. L'ingegneria tissutale offre un'alternativa promettente e biocompatibile. Questa tesi di laurea magistrale esplora lo sviluppo di hydrogel di PEG (polietilenglicole) composti da PEG-4MAL e due crosslinker, VPM e PEG-diSH, utilizzati in rapporto 50:50. Gli hydrogel contenenti il peptide VPM, degradabile dalle metalloproteasi (MMPs), combinato con PEG-diSH, risultano in un tasso di degradazione controllato degli hydrogel del 50%.
Queste strutture 3D sono state ulteriormente arricchite con RGD (una sequenza di adesione cellulare) e composti di boro come il Bortezomib, con l'obiettivo di attivare i trasportatori di boro NaBC1 e le integrine presenti sulla superficie delle cellule. Questa attivazione favorisce l'adesione cellulare, la proliferazione e la differenziazione.
Questo progetto di tesi di laurea si è principalmente concentrato sull'analisi delle proprietà fisico-chimiche e della biocompatibilità del materiale. Lo studio ha coinvolto diversi setup sperimentali: PEG puro, PEG-RGD, PEG-RGD-Boro e PEG-RGD-Bortezomib.
Sono stati eseguiti saggi di swelling per misurare la capacità di assorbimento d'acqua e la stabilizzazione fisica nel tempo.
I saggi di degradazione sono stati invece in seguito effettuati per valutare la degradazione enzimatica degli hydrogel (dovuta al VPM).
Test reologici utilizzando un reometro ibrido hanno valutato le proprietà visco-elastiche attraverso sweep di deformazione e frequenza.
La biocompatibilità è stata poi verificata in vitro utilizzando un saggio MTS con due linee di fibroblasti umani, misurando la vitalità cellulare e la tossicità del materiale stesso.
Infine, sono stati condotti test in vivo utilizzando uova fecondate, valutando la vascolarizzazione attraverso l'analisi dell'angiogenesi.
Questo lavoro fa parte di un più ampio progetto di ricerca che ha come obiettivo principale lo studio della rigenerazione muscolare. Ulteriori esperimenti potrebbero coinvolgere la verifica dell'effettiva adesione, proliferazione e differenziazione cellulare.
Questo campo dell'ingegneria tissutale ha un grande potenziale per la rigenerazione muscolare, offrendo soluzioni per condizioni attualmente incurabili.

Chapter 1

Introduction

1.1 Overview

This master thesis work was developed with Dr.Rico Tortosa's research team at the Universitat politècnica de València (UPV), in particular at the Centro de Biomateriales e Ingeniería Tisular (CBIT), while supervised by Professor Brusatin at the University of Padova (Unipd), from the Department of Industrial Engineering (DII).
This research project involved different disciplinary fields including tissue engineering, materials engineering, biology and biotechnology.

Figure 1.1: Centro de Biomateriales e Ingeniería Tisular (CBIT) at the Universitat politècnica de València (UPV).

Figure 1.2: From left to right: Rodriguez Romano, myself (Martina Ferrara), and Dr Gonzalez Valdivieso at the CBIT

1.2 Aim and goals of the project

The aim of this master thesis project was to develop an hydrogel specifically designed for muscular regeneration. This work is a component of a broader research initiative focused on ensuring that, through the injection of a specific biomaterial, the adhesion, proliferation, and differentiation of muscle cells can be effectively achieved. The overarching goal of the larger project is to address muscular injuries, whether they result from trauma or more severe conditions such as pathological dystrophies (for example the Duchenne dystrophy).

This particular thesis concentrated primarily on examining the physico-chemical characteristics and the biocompatibility of the hydrogels when interacting with human fibroblasts. These aspects are crucial because understanding the material's physical and chemical properties, as well as its compatibility with living tissues, lays the groundwork for future applications in muscle regeneration.

The physico-chemical characteristics refer to the hydrogel's structure, chemical composition and mechanical properties. These factors determine how the material interacts with cells and the surrounding environment, influencing its ability to support the repair of muscle tissue. By analyzing these properties, the research aims to ensure that the hydrogel has the necessary qualities to function effectively within the human body.

Biocompatibility, on the other hand, is essential for ensuring that the hydrogel does not elicit adverse immune responses when introduced into the body. In this research, particular attention was given to how human fibroblasts, respond to the hydrogel. Positive biocompatibility results are indicative of the hydrogel's potential to integrate seamlessly with human tissues, which is a critical step towards its use in clinical settings.

If these preliminary studies on biocompatibility and physico-chemical properties yield positive results, the hydrogel could then be tested further in future experiments aimed at muscular regeneration. The ultimate vision is for this hydrogel to be utilized in clinical treatments to repair damaged muscle tissues, providing a less invasive alternative to current surgical techniques and potentially improving the quality of life for patients suffering from degenerative muscle diseases.

In summary, this thesis represents a significant step in the development of advanced materials for regenerative medicine, with a specific focus on applications in muscle repair. Through meticulous analysis and testing, this research seeks to pave the way for new, effective treatments for muscle injuries and diseases, contributing to the broader field of biomedical engineering and tissue regeneration.

Chapter 2

State of the art

2.1 The muscular tissue and its pathologies

Striated muscle includes two primary muscle categories: skeletal and cardiac. Whereas cardiac muscle embodies a collection of self-stimulating, enduring muscle cells with a moderate energy demand, skeletal muscle consists of innervated, voluntary muscle cells tending to fatigue and demanding high energy inputs. A superficial examination of cellular architecture and intercellular communication reveals the intricate nature of striated muscle, tailored to facilitate contraction, force generation and motion [1].
Skeletal muscle represents a meticulously organized tissue comprising numerous bundles of muscle fibers (myofibers). Each myofiber, containing numerous myofibrils, represents a muscle cell characterized by the fundamental sarcomere as its basical cellular unit. Fascicles, clusters of myofibers, form the structural components, with layers of fascicles ultimately building muscle tissue, sequentially enveloped by the extracellular matrix and upheld by cytoskeletal frameworks. Abundantly vascularized and innervated, skeletal muscle hosts metabolic and regulatory apparatuses that facilitate proficient energy generation and cellular equilibrium [2].

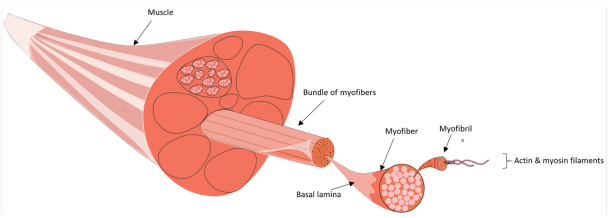

Figure 2.1: Representation from [2] of the skeletal muscle made of myofibers: each one is surrounded by basal lamina, contains arrays of myofibrils and includes actin and myosin microfilaments.

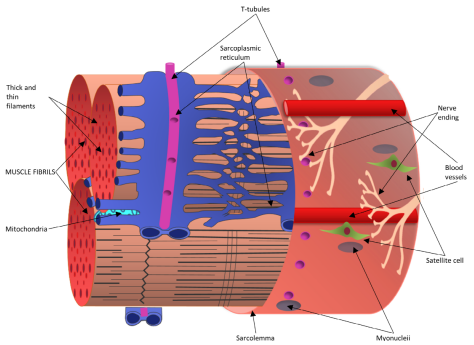

Figure 2.2: A schematic portrayal from [2] of a skeletal muscle fiber which depicts a mature muscle fiber as a cluster of myofibrils enveloped by the sarcolemma.

Sarcomeres are a complex molecular structure composed of two main types of protein filaments: thin filaments made of alpha-actin and associated proteins, and thick filaments made of myosin and its associated proteins, aligned parallel to the muscle fiber axis. Each sarcomere is bounded by Z-disks, which separate the lighter I band spanning adjacent sarcomeres. At the center of the sarcomere is the dense A-band, primarily made up of thick filaments, with a lighter H-zone in the middle. The M-line runs through the H-zone, providing structural support. Thin filaments are anchored at the Z-disk, while the M-band links the thick filaments. Muscle contraction starts when troponin-C binds to Ca2+ ions released during Excitation-Contraction Coupling (ECC) [3].

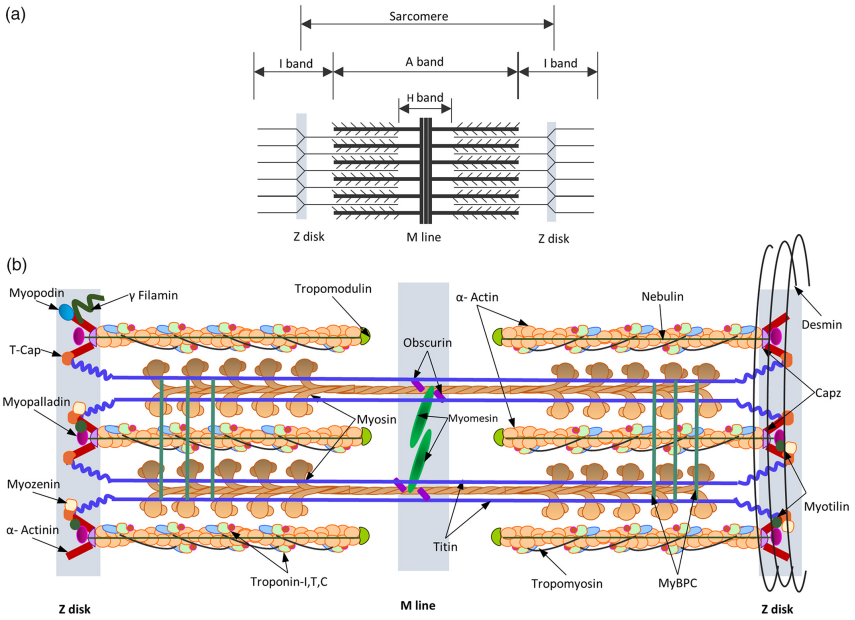

Figure 2.3: A schematic depiction from [3] of the sarcomere in striated skeletal muscle which illustrates the layout of thick and thin filaments, while also pinpointing the regions of overlap between them.

The harmonious interplay among these constituents is indispensable for maintaining muscular well-being and associated motor functions. Disruptions to this equilibrium lead to muscle deterioration, characterized by decreasing muscle fibers, diminished motor performance and, in severe instances, mortality. [1]
Injuries deriving from sports, household accidents, or even vehicular collisions with moderate to severe consequences, often necessitate surgical interventions, such as the insertion of muscle flaps and composite tissue grafts. There are two main possible approaches that represent nowadays a possible solution. The first one involves harvesting muscle fragments along with their accompanying nerve and blood supply from the patient's own tissues for transplantation to the affected area (autologus transplant). However, this method is constrained by the limited availability of donor tissue without risking harm to the donor site, rarely resulting in complete functional recovery and occasionally culminating in fibrosis rather than muscle regeneration. Alternatively, the second method employs allografts: transplantation of skeletal muscle, skin, bone, and tendon from a genetically distinct

donor. Here, compatibility and possible rejection represent a significant challenge, potentially triggering an exaggerated immune response in the recipient, necessitating ongoing immunosuppressive therapy. Conversely, irregularities in the arrangement of muscle fibers manifest as myopathies, leading to muscle atrophy or degeneration. Conditions such as muscular dystrophies (e.g., Duchenne and Becker) and spinal muscular atrophy (SMA) are genetic neuromuscular disorders.

In muscular dystrophies, in particular, mutations in genes that directly affect muscle tissue lead to muscle cell atrophy and loss.

As novel pathological mechanisms emerge, various therapeutic approaches, notably tissue engineering, are under exploration [4].

2.2 The ECM, its components and interactions

2.2.1 ECM

Each different tissue is characterized by the Extracellular Matrix (ECMs), which represents an intricate and well-organized three-dimensional architectural network that plays critical structural and functional roles in tissue organization, remodeling and cellular processes regulation. This ultrastructure is composed of various building blocks, including collagens, proteoglycans (PGs) and glycosaminoglycans (GAGs), elastin and elastic fibers, laminins, fibronectin, and other proteins/glycoproteins such as matricellular proteins [5]. Acting as communication links between cells within organs and tissues, the ECM coordinates multiple signaling pathways, both inside-out and outside-in, thereby guiding tissue morphogenesis, development, and homeostasis. The ECM also regulates cellular physiology, growth, survival, differentiation and adhesion. During pathological conditions, the ECM undergoes extensive remodeling, playing significant roles in driving disease progression [6].

Different tissue types (e.g., epithelial, nervous, muscle, and connective tissues) possess specific ECM phenotypes tailored to meet the requirements for optimal tissue functions. However, ECM composition can be dynamically adjusted in response to biochemical or mechanical signals, facilitating a finely-tuned remodeling process. Proteoglycans (PGs), composed of a protein core adorned with negatively charged GAGs play crucial structural and biological roles. They contribute to tissue mechanical resistance to compression and hydration, and also serve to sequester growth factors (GFs) within the ECM. PGs are categorized into four groups based on their localization and homology [7].

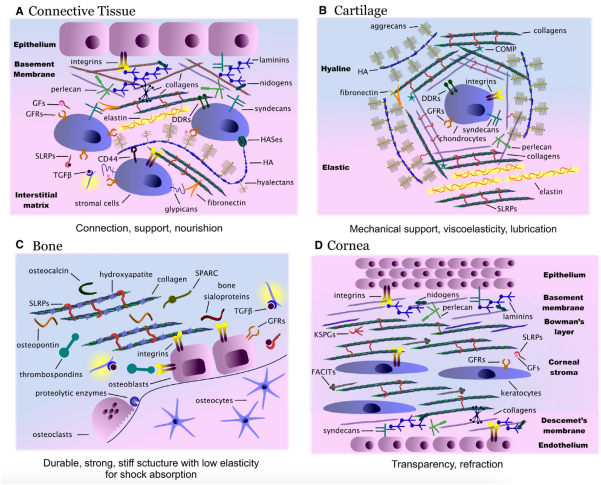

Figure 2.4: Schematic representation from [6] of the composition and structure of ECMs loose connective tissue (A), and specialized connective tissues such as cartilage (B), bone (C) and cornea (D)

2.2.2 Fibronectin

Fibronectin (FN) is a glycoprotein present in the ECM and in the blood plasma. It has a size ranging from 230 to 270 kDa, typically existing as a dimer connected by disulfide bonds at the C-termini. Each monomer comprises three types of repeating units: 12 Type I, 2 Type II, and 15–17 Type III domains, together making up 90% of the FN sequence. An example of these domains is the RGD sequence (further deepened in the paragraph below) [8].

This macromolecule forms supramolecular assemblies and regulates mechanical properties, such as tension due to conformational changes of its fibers; active-stretching versus relaxed fibronectin fibers.

Fibronectin also interacts with integrins regulating cellular adhesion, as well as with GFs, cytokines, and ECM molecules.

In general, it plays a crucial role in various biological processes, including: wound healing, embryogenesis, blood coagulation, cell adhesion, cell migration and cell differentiation [7].

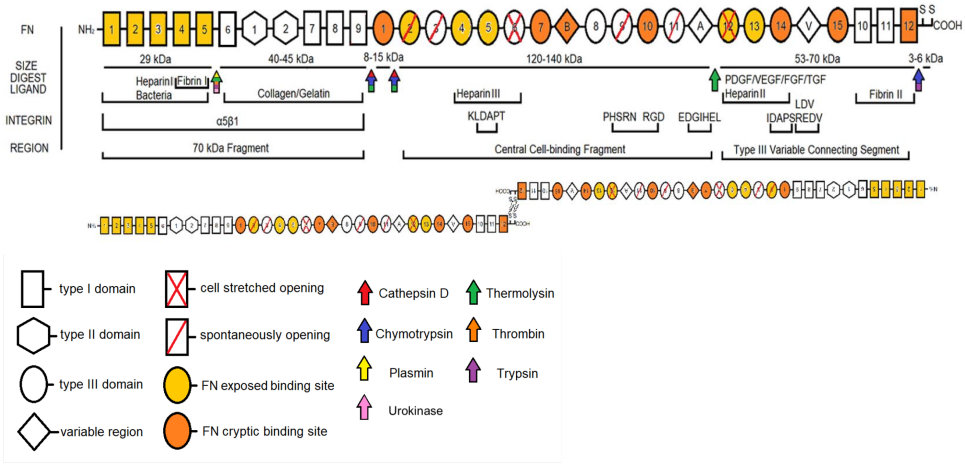

Figure 2.5: Schematic representation from [8] of the composition and the principal domains of the fibronectin

2.2.3 RGD sequence

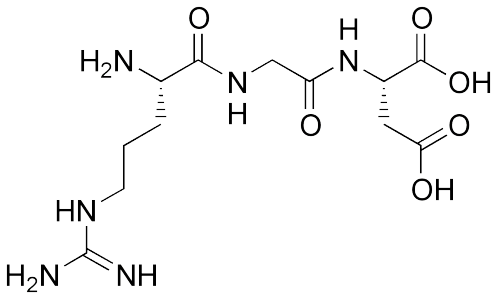

Figure 2.6: Schematic representation of the chemical composition of the RGD sequence from [9]

The arginine-glycine-aspartic acid (RGD) cell adhesion sequence was first identified in fibronectin over 12 years ago by Pierschbacher and Ruoslahti (1984).
This observation was quickly validated for fibronectin and subsequently extended to other proteins. This protein is essentially made of three amminoacids: Arginine (R), Glycine (G) and Aspartic Acid (D) and it was revealed that the RGD sequence serves as the cell attachment site for many adhesive proteins. These findings, along with the subsequent identification of integrins-cell surface receptors that recognize the RGD sequence in various proteins, have confirmed the RGD as an element of significant importance in cell adhesion biology, serving as the prototype adhesion signal. Furthermore, RGD has emerged in numerous pharmaceutical applications [9].
Due to its compact structure, the RGD site can be easily replicated using peptides, which was the method originally used to identify it. Short peptides containing the RGD sequence can mimic cell adhesion proteins in two ways: when coated onto a surface, they promote cell adhesion, whereas when in solution, they act as decoys, preventing adhesion.
RGD peptides that have not been specifically designed to selectively bind certain integrins, mimic multiple adhesion proteins and can bind to more than one receptor [10].
The conformation of the amino acids is also crucial: a peptide in which the aspartic acid is in the D-form is inactive. However, RGD peptides containing a D-arginine residue are active. The smallest active unit in these peptides is the RGD sequence itself.
Initially, the fibronectin cell attachment site was defined as a tetrapeptide because this was the smallest peptide with measurable activity. However, it was recognized that while the RGD sequence had to remain unchanged for cell attachment activity to be preserved, the amino acid following this sequence (a serine in fibronectin) could vary.
The principal role of the RGD sequence in cell recognition was first deduced from the observation that not only did a fibronectin receptor, later named $\alpha 5\beta 1$, bind to its ligand in an RGD-dependent manner, but so did another protein with a similar polypeptide composition to the fibronectin receptor, which bound to vitronectin instead of FN [11].
The RGD sequence is recognized by at least 8, and potentially up to 12, of the currently known 20 or so integrins in their ligands.

2.2.4 Integrins

Integrins are heterodimeric proteins composed of subunits which guarantee the specificity of the ligand and contain potential binding sites for the ligand. In each case, the ligand-binding site is at or near a binding site for divalent cations.
Initial studies involving fibronectin fragments and peptides with structural constraints suggested that the presence of the RGD sequence within RGD proteins played a crucial role in their recognition by integrins [9].
Integrins, the primary transmembrane mechanosensors responsible for linking the extracellular matrix (ECM) to the intracellular cytoskeleton, are subject to bidirectional regulation by both intracellular and extracellular signals, leading to the formation of focal adhesions. Within skeletal muscle, $\beta 1$ integrin and its associated partners ($\alpha 1$, $\alpha 3$, $\alpha 4$, $\alpha 5$, $\alpha 6$, $\alpha 7$) play crucial roles in regulating myogenic gene expression, migration, fusion, and muscle stability, while $\alpha \mathrm{v} \beta 3$ is implicated in muscle regeneration, serving as a key component of focal adhesions in myoblast precursor cells. Moreover, $\alpha \mathrm{v} \beta 3$ is essential for maintaining Rac1 activity in differentiated myoblasts, thereby promoting myogenesis.
Skeletal muscle integrins interact with the muscle ECM, primarily composed of laminin family members, fibronectin, proteoglycans, and collagen IV family members. Among these ECM components, fibronectin stands out as a multifunctional protein that undergoes significant cell upregulation following muscle injury, causing a substantial influence on supporting the proliferation and differentiation of satellite cells during the repair process. [12]

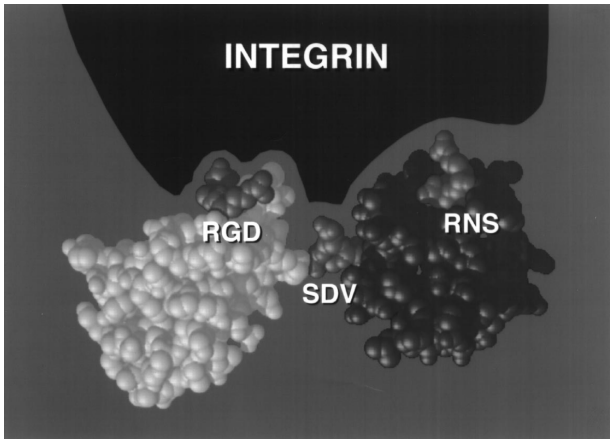

Figure 2.7: A model from [9] for the recognition of the fibronectin RGD site and auxiliary sites by an integrin.

2.3 Tissue engineering and existing solutions

Tissue engineering strives to fabricate scaffolds that integrate cells with varying differentiation capacities, aiming to mimic the natural tissue environment, principally represented by the ECM (which was described above) and the signals that regulate cell growth and differentiation. In essence, this interdisciplinary approach seeks to regenerate functional organic tissues without eliciting adverse reactions within the organism [4].
Before deepening on the already existing materials that can be applied in tissue engineering, a premise must be made regarding the muscular regeneration and improvement.
An example of an already utilized element applied as muscular integrator by athletes is creatine.
In particular, creatine emerges as a favored nutritional ergogenic aid among athletes. Researches demonstrated that supplementing with creatine elevates intramuscular creatine levels, potentially clearifying the observed enhancements in high-intensity exercise performance, leading to greater training adaptations.
Various clinical investigations have explored the potential applications of creatine supplementation in managing neurodegenerative conditions (such as muscular dystrophies, Parkinson's and Huntington's disease), diabetes and many other conditions [13].

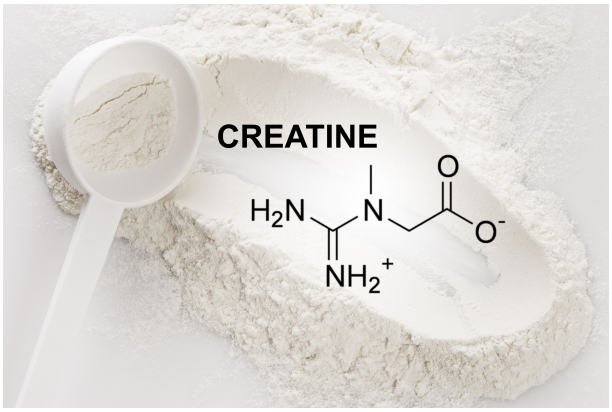

Figure 2.8: Chemical structure of the creatine from [13] usually assumed by athletes in the form of powder to be diluted.

On the other hand, stem cells, particularly the ones obtained from the bone marrow, stand out as promising candidates for tissue repair. Despite not directly evolving into muscle cells, their notable effects and fusion with myoblasts, during myotube formation, highlight their significance based on their predisposition towards the myogenic lineage.
Nevertheless, while stem cells own the capacity to release growth factors, incorporating bioactive molecules into the muscle analog may prove necessary to guarantee the resilience of vascular and neuronal networks post-implantation [14].

2.4 Biomaterials

Various biomaterials have been investigated for skeletal muscle regeneration, with the main aim being that the biomaterial itself catalyzes skeletal muscle [15].
In general, considering the kinetics of degradation of the utilized biomaterial, is crucial in tissue engineering approaches.
There are two main situations in which these biomaterials could be applied.

Ideally, biomaterials supporting non-myogenic stem cells should exhibit a mild to fast degradation rate. Non-myogenic stem cells are anticipated to contribute to intrinsic muscle regeneration through paracrine effects and by merging with myoblasts during myotube formation, thus actively participating in the inflammation and regeneration phases of skeletal muscle regeneration. Once cellular regenerative activity is accomplished, the biomaterial's role diminishes, making its support no longer necessary.
On the other hand, biomaterials supporting myogenic cells should have a delayed degradation rate. Cells possessing myogenic potential not only initiate myogenesis, but also undergo differentiation, culminating in the formation of myofibers [16].

Consequently, these cells contribute to the regenerative process and simultaneously they hold the capability to replace the lost tissue. In particular, regarding the context of supporting skeletal muscle analogs, the biomaterial should exhibit a slow degradation rate, gradually breaking down during the remodeling phase of skeletal muscle regeneration [17].

Biomaterials, particularly hydrogels, have been designed and employed to present specific subsets of mechanical, structural, and compositional cues, enabling investigations into numerous cellular processes crucial for understanding morphogenesis, aging, and disease progression. There is a pressing need for culture systems that better replicate the biological environment, connecting the gap between conventional cell cultures and the intricate native in vivo environments. The field of biomaterials continues to make steps forward in introducing such complexity into cell culture systems, offering means to precisely control the mechanical, compositional, and structural characteristics. This advancement enables the creation of culture environments that more precisely mirror the features of native tissues, deepening into cellular behavior and responses.[18]

A big range of biomaterials has been used for skeletal muscle repair comprising ECM derivatives (such as collagen, fibrin or gelatin) poly-saccharides (like hyaluronic acid HA, chitosan, keratin, alginate), matrices that have been decellularized or synthetic biomaterials (like PGA, PLA, PLGA) [19] [20]. A large majority of strategies for functionalizing the biomaterial matrices rely on the delivery of growth factors (GFs) or other small bioactive molecules [21] [22]. However, scarce reports describe material systems for ion-delivery to stimulate intracellular signaling [23] [24].

Nevertheless, there remains a critical need to innovate new methods and materials that effectively promote the repair and functional regeneration of skeletal muscle. In pursuit of this objective, a diverse array of biomaterial systems has been developed. These include patterned glass substrates, elastomeric films, hydroxyapatite ceramics, and fibrillar foams, each offering unique properties and functionalities tailored to address specific challenges associated with skeletal muscle repair.
These biomaterial platforms hold promise for advancing the field of muscle tissue engineering by providing versatile tools to support and guide the regeneration of damaged muscle tissue towards functional recovery.[25]

Therefore, naturally biodegradable polymers, such as collagen degraded by collagenase or hyaluronic acid (HA) degraded by hyaluronidase, will degrade more rapidly compared to those solely susceptible to hydrolysis, such as gellan gum or PEG.
Therefore, biomaterials have been shaped into bundle-like scaffolds or fibrillar structures to encourage aligned cellular orientation, mirroring the natural organization of skeletal muscle. Natural polymers present an intresting avenue, as they present intrinsic cell adhesive motifs. Collagen and fibrin have emerged as the most extensively studied biomaterials for facilitating cell growth, while other natural biomaterials like hyaluronic acid and laminin have also gained attention in research.

In summary, the various array of available natural biomaterials, coupled with different processing techniques, has sparked innovative designs aimed at favouring the support that biomaterials try to guarantee for cells. Incorporating cell adhesive cues, biodegradability, porosity, electroactivity, and alignment-inducing cues has been essential in facilitating the adhesion, proliferation, differentiation, and organization of cells. Particularly, while biomaterial rigidity is a critical feature, it has often been overlooked in these studies. These attributes should be carefully integrated into tissue engineering strategies, considering the use of myogenic or non-myogenic stem cells, to optimize skeletal muscle regeneration dynamics [26].

2.4.1 Naturally derived materials

Polimers made of naturally derived materials have often been used in tissue regeneration applications because they recall macromolecular properties similar to the natural ECM or even they actually are its components.
Similarly, HA is found in varying amounts in all tissues of adult animals [27]. Like HA, alginate and chitosan are hydrophilic linear polysaccharides [28]. They have also been shown to interact in a favorable manner in vivo and thus have been utilized as hydrogel scaffold materials for tissue engineering [29].

Collagen is an attractive material for biomedical applications as it is the most abundant protein in mammalian tissues (it represents the 25% of the total protein mass of most mammals).
Collagens are the predominant constituents of ECMs, accounting for over 30% of their composition.
Among collagens, types I, II, and III are particularly abundant, comprising 80–90% of total body collagen.
Collagens are characterized by their characteristic triple-helix morphology, formed by homo- or hetero-trimeric chains.
These chains are held together by hydrogen and covalent bonds, imparting stability. Additionally, collagen strands can self-aggregate, forming stable fibers critical for tissue strength and integrity [30].
They serve as supportive tissue material while also imparting elasticity and stability. The collagen family comprises 28 members, classified into various subfamilies based on their supramolecular structure and functions [31].

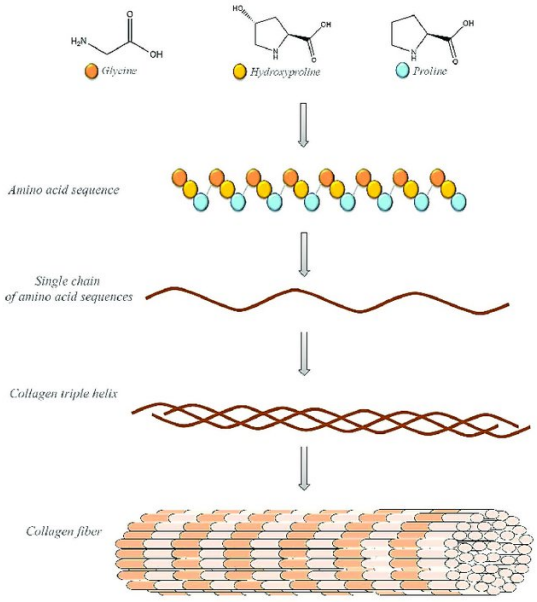

Figure 2.9: Representation from [31] of the structure of a fiber of Collagen

Moreover, collagen fibers and scaffolds can be created and their mechanical properties improved by introducing various chemical crosslinkers (i.e. glutaraldehyde, formaldehyde, carbodiimide), by crosslinking with physical treatments (i.e. UV irradiation, freeze-drying, heating), and by blending it with other polymers (i.e. HA, PLA, poly(glycolic acid) (PGA), poly(lactic-co-glycolic acid) (PLGA), chitosan, PEO) [32] [33] [34] [35].
Collagen undergoes natural degradation mediated by metalloproteases, particularly collagenase, and serine proteases. This enzymatic degradation mechanism enables local control of collagen breakdown by cells within the engineered tissue.

Hyaluronic acid (HA), on the other hand, represents the most basic glycosaminoglycan (GAG) and is ubiquitous in nearly all mammalian tissues and fluids [27].
HA contributes significantly to water retention in tissues and helps maintain their structural integrity. It plays a fundamental role in various physiological processes such as embryogenesis, tissue repair, regeneration, and homeostasis. HA exhibits versatile functions depending on factors such as its size, concentration, interactions with cell receptors and binding partners within the ECM. Additionally, HA can regulate signaling pathways in a context- and tissue-specific manner [36].
In addition to its abundance during wound healing and its presence as a major component of synovial fluid in joints, hyaluronic acid (HA) is a linear polysaccharide composed of repeating disaccharide units.

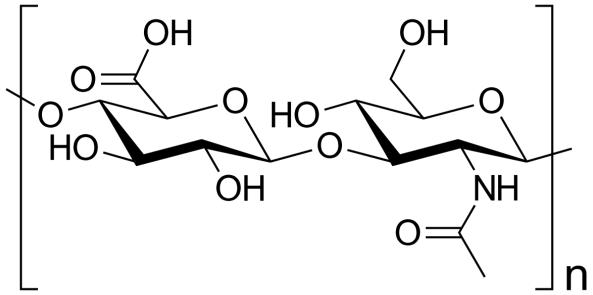

Figure 2.10: Representation of the chemical structure of HA from [36]

Hydrogels derived from HA are created using diverse methods, such as covalent crosslinking with hydrazide derivatives, esterification, and annealing processes [37].
Moreover, HA has been combined with both collagen and alginate to form composite hydrogels. Hyaluronic acid (HA) undergoes natural degradation by hyaluronidase, allowing cells in the body to regulate the localized clearance of this material [38].

Alginate, on the other hand, has found extensive use in various medical applications, including cell encapsulation and drug stabilization and delivery. This is attributed to its ability to gel under gentle conditions, low toxicity, and widespread availability. Alginate is a linear polysaccharide copolymer composed of (1–4)-linked -D-mannuronic acid (M) and -L-guluronic acid (G) monomers, primarily derived from brown seaweed and bacteria.
Within the alginate polymer, the M and G monomers are arranged in either repeating or alternating blocks. The composition and distribution of each monomer vary depending on the species, location, and age of the seaweed from which the alginate is sourced [39]. Gels are formed when divalent cations such as Ca2+, Ba2+, or Sr2+ cooperatively interact with blocks of G monomers to form ionic bridges between different polymer chains. The crosslinking density and thus mechanical properties and pore size of the ionically crosslinked gels can be readily manipulated by varying the M to G ratio and molecular weight of the polymer chain. Gels can also be formed by covalently crosslinking alginate with adipic hydrazide and PEG using standard carbodiimide chemistry [40] [41]. Ionically crosslinked alginate hydrogels do not own a specific kinetic of degradation, but go through an uncontrolled dissolution. Mass is depleted via the process of calcium ion exchange, succeeded by the dissociation of individual chains. This sequential phenomenon ultimately leads to a decline in mechanical stiffness as time progresses [42]. Hydrolytically degradable variants of alginate have been engineered through a process involving partial oxidation of both alginate and its derivative, polyguluronate. This process produces oxidized alginate and poly(aldehyde guluronate) (PAG), respectively [43].

Chitosan has gained attention in numerous tissue engineering projects due to its structural resemblance to naturally existing glycosaminoglycans (GAGs) and its susceptibility to enzymatic degradation in humans. Derived from chitin, which is prevalent in arthropod exoskeletons, chitosan is a linear polysaccharide comprising (1–4)-linked d-glucosamine and N-acetyl-d-glucosamine residues [44]. Chitosan exhibits solubility in weak acids, which protonate its free amino groups. Upon dissolution, chitosan can undergo gelation through pH elevation or extrusion into a nonsolvent [45]. Chitosan derivatives and composites have been effectively gelled through various methods, including glutaraldehyde crosslinking, UV irradiation and thermal adjustments. Lysozyme-mediated degradation affects chitosan, with degradation kinetics inversely correlated to its degree of crystallinity [46].

A last interesting naturally derived material is electrospun fibrin bundles.
These have demonstrated the ability to promote the alignment of myoblasts in vitro and increase myofiber density in vivo, attributed to the inherent alignment and stiffness of the electrospun scaffold [47].

2.4.2 Hydrogels

Hydrogels, water-swollen networks of polymers, have emerged as highly promising options for cell culture due to their ability to mimic key aspects of native extracellular matrices (ECMs). With mechanics similar to many soft tissues and the capacity to support cell adhesion and protein sequestration, hydrogels offer a versatile platform for cell culture applications. Their utility extends across a broad spectrum of cell culture efforts, enabling the deepening of fundamental phenomena governing cell behavior and facilitating the expansion and directed differentiation of diverse cell types. In contrast to conventional culture substrates, hydrogels provide unique capabilities that push researchers to explore and manipulate cellular processes with unprecedented precision and control [25].

Hydrogels exhibit variations in size, architecture and functionality, collectively influencing their suitability for drug delivery applications. Within hydrogel structures, features span a wide range of length scales, from centimeters to sub-nanometers. The macroscopic design primarily determines the delivery routes feasible for hydrogels within the human body, as they can be shaped into nearly any desired size and form. The presence of micropores within hydrogels significantly impacts their overall physical properties, such as deformability, while facilitating convective drug transport [48].

At the nanometer scale, a cross-linked polymeric network envelops the water contained within the hydrogel matrix, contributing to its structural integrity and drug release characteristics. In hydrogel networks, open spaces exist, characterized by the mesh size of the network. This mesh size profoundly influences the diffusion of drugs within the hydrogel matrix. Moreover, at the molecular and atomistic levels, various chemical interactions may occur between drugs and polymer chains. Polymer chains offer numerous binding sites for interactions with drugs, which can be custom-made through a variety of physical and chemical strategies. The features at both the mesh scale and the molecular and atomistic scale play pivotal roles in controlled drug release. Importantly, these features are often decoupled from the macroscopic properties of the hydrogel, allowing for independent design optimization at each length scale. This multiscale nature enables the modular design of hydrogels, providing a versatile platform to meet specific application-based requirements[49].

While certain design criteria are universal across all hydrogel delivery systems, others are thought for specific therapeutic applications. Overall, the fabrication of hydrogel delivery systems must prioritize the preservation of drug bioactivity. Additionally, both the drug and hydrogel must maintain chemical and physical stability throughout packaging, transport, and storage processes. Hydrogels can be inserted through various methods, including surgical implantation, local needle injection, or systemic delivery

via intravenous infusion. The selection of a delivery method depends on optimizing overall efficacy and ensuring patient compliance, considering factors such as the nature of the drug, the targeted tissue or organ, and the desired treatment outcome. The methodology in which the hydrogel releases the drug often dictates the achievement of desirable therapeutic outcomes. Factors such as the required duration of drug availability (short-term versus long-term) and the desired release profile (continuous versus pulsatile) are dependent on the specific application at hand. Upon exhaustion of the drug payload, the hydrogel should be designed to either degrade to facilitate removal, or be capable of being refilled for reuse [50].

Moreover, the degradation kinetics of the hydrogel may need to be tailored to synchronize with tissue regeneration processes. In addition to these general requirements, application-specific demands further shape hydrogel design considerations. For instance, in the treatment of skin wounds, hydrogels are applied to dynamic surfaces, necessitating adhesiveness and conformability to ensure effective wound coverage [51].

Furthermore, they must possess sufficient toughness to withstand surface movement, such as the strain induced by knee bending up to 50%, as well as environmental stressors like compression and scratching. Meeting these diverse application-based requirements underscores the versatility and adaptability of hydrogel-based delivery systems in addressing complex therapeutic challenges [52].

Hydrogels that can be applied in the tissue engineering scaffolds field, can be produced through a variety of synthetic and naturally derived materials. The first ones include: poly(ethylene oxide) (PEO), poly(vinyl alcohol) (PVA), poly(acrylic acid) (PAA), poly(propylene furmarate-co-ethylene gly-col) (P(PF-co-EG)) and polypeptides. The naturally derived polymers, instead, comprehend: agarose, alginate, chitosan, collagen, fibrin, gelatin, and hyaluronic acid (HA) [53].

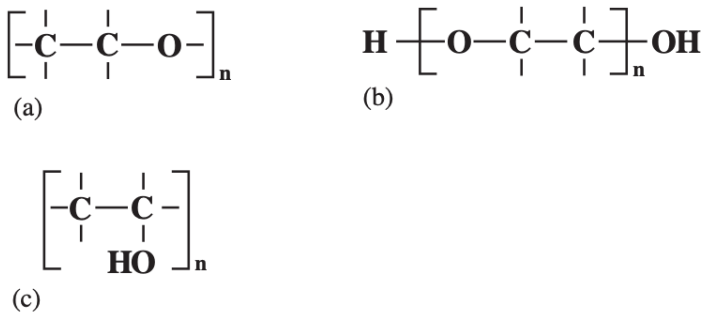

Figure 2.11: Formulas of a) PEO b) PEG c) PVA from [53]

2.4.3 Synthetic materials

Synthetic hydrogels hold great appeal in tissue engineering due to their controllable and reproducible chemistry and properties. For instance, synthetic polymers offer the advantage of being produced with specific molecular weights, block structures, degradable linkages, and crosslinking modes in a reproducible manner. These properties, in turn, govern crucial aspects such as gel formation dynamics, crosslinking density, and mechanical and degradation characteristics of the material. As already mentioned above, examples of such synthetic materials include PEO, PVA and poly(poly(ethylene glycol) fumarate-co-ethylene glycol) (P(PF-co-EG)).

PEO, in particular, has garnered attention as one of the most commonly utilized synthetic hydrogel polymers in tissue engineering applications.
Notably, PEO has received FDA approval for various medical applications, underscoring its safety and suitability for clinical use in tissue engineering and regenerative medicine. PEO and its chemically analogous counterpart, poly(ethylene glycol) (PEG) are hydrophilic polymers capable of photocrosslinking by introducing acrylate or methacrylate groups at each end of the polymer chain [54].
Upon mixing the modified PEO or PEG with the suitable photoinitiator and subjecting them to UV exposure, hydrogels are formed through crosslinking reactions. Additionally, thermally reversible hydrogels have been developed using block copolymers of PEO and poly(l-lactic acid) (PLLA), as well as PEG and PLLA. These innovative materials offer the advantage of undergoing reversible gelation upon changes in temperature, thereby enabling dynamic control over their physical properties for various biomedical applications. In addition to thermally reversible hydrogels, degradable PEO and PEG hydrogels have been developed using block copolymers containing hydrolytically degradable poly(lactic acid) (PLA) segments and enzyme-specific cleavage sequences of oligopeptides.
These innovative materials offer the advantage of controlled degradation, making them suitable for various biomedical applications [55].

Another synthetic hydrophilic polymer profoundly investigated for space-filling and drug delivery applications is PVA. PVA hydrogels can be physically crosslinked through repeated freeze-thawing cycles of aqueous polymer solutions or chemically crosslinked using agents such as glutaraldehyde, succinyl chloride, adipoyl chloride, and sebacoyl chloride. Moreover, PVA can be blended with other water-soluble polymers and crosslinked either physically or chemically, resulting in hydrogels with enhanced properties and functionalities [56].Furthermore, a novel synthetic hydrogel block copolymer, P(PF-co-EG), has been developed as an injectable carrier for bone and blood vessel engineering applications. This innovative material offers exciting possibilities for tissue engineering by providing a versatile platform for delivering therapeutic agents and promoting tissue regeneration [53].

2.4.4 PEG Hydrogels and crosslinkers

Non-ionic and hydrophilic PEG gel systems are gaining significance in the world of tissue engineering. In recent decades, poly(ethylene glycol) (PEG) hydrogels have been widely employed as matrices for regulating drug delivery and as carriers for cell delivery to facilitate tissue regeneration [57]. The adaptability of PEG macromer chemistry, coupled with its outstanding biocompatibility, has pushed the advancement of numerous intricately designed hydrogel systems for use in regenerative medicine. Many of these investigations have brought promising outcomes in both experimental and clinical settings. Within the domain of controlled delivery, meticulously crafted PEG hydrogels play a pivotal role in orchestrating vital cellular processes such as viability, proliferation, secretion, and differentiation. There is a duality in objectives and guiding principles in this context: firstly, to achieve localized and sustained release of therapeutics for heightened effectiveness, and, secondly, to alleviate adverse reactions while preserving the bioactivity of the encapsulated therapeutics. Fulfilling these objectives demands careful deliberation of several factors, including: the physiological environment of target tissues, mechanisms governing gelation and molecule loading/unloading, molecular characteristics of the therapeutics and potential interactions with the polymeric hydrogels. PEG hydrogels offer a distinct advantage for cell encapsulation owing to their remarkable biocompatibility under suitable polymerization conditions [58].

By copolymerizing with other macromolecules, various functional groups can be easily incorporated to either inhibit or improve cell survival and activity. For instance, the integrin binding peptide Arg-Gly-Asp (or RGD) is frequently added as a pendant functional group within otherwise biologically inert PEG hydrogels to enhance the survival of cells reliant on adhesion, such as osteoblasts [59].

Although PEG hydrogel environments typically facilitate easy diffusion of nutrients, this characteristic often poses challenges for localized delivery and therapeutic efficacy of soluble factors aimed at the encapsulated cells. This is because the inert gel networks allow equal permeability to co-encapsulated therapeutics. Therefore, the manner in which bioactive molecules are presented to encapsulated cells within PEG hydrogel networks, temporally and spatially present a significant challenge in the design of hydrogel delivery systems and remains a focus of intense research. Various methods of gelation, including physical, ionic, or covalent interactions, can be employed to form PEG gels.
However, chemically or covalently crosslinking results in relatively stable hydrogel structures with adjustable physicochemical properties such as permeability, molecular diffusivity, equilibrium water content, elasticity, modulus and degradation rate.
Additionally, integrating degradable linkers into the covalent crosslinks enables the fabrication of well-defined network structures with tunable properties over time [60].

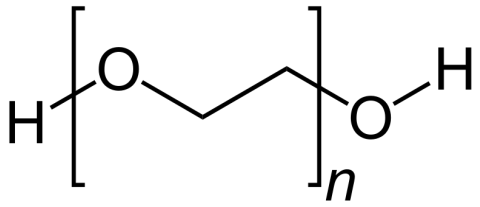

Figure 2.12: PEG chemical structure from [60]

Deepening the PEG material, a loosely crosslinked PEG hydrogel can readily retain more than 95% of water within its total mass. This high water content mimics natural soft tissue, thus providing a conducive environment for numerous encapsulated biomolecules and cells. This characteristic is crucial for tissue regeneration as it facilitates easy exchange of nutrients and waste, thereby supporting long-term viability of cells and tissues. Moreover, PEG hydrogels possess a beneficial anti-fouling property, which inhibits non-specific protein adsorption and cell adhesion. This feature helps maintain the integrity of the hydrogel and prevents unwanted interactions with surrounding biological components, enhancing its suitability for various biomedical applications [61] [62].

This property is intriguing as it helps the creation of functional patterns either on PEG surfaces or within three-dimensional PEG hydrogels, when modified with appropriate adhesion molecules.
Similar to the high water-content property of PEG hydrogels, the ability of PEG molecules to prevent non-specific biomolecular interactions has its advantages and disadvantages. For tissue regeneration, the anti-fouling property of PEG hydrogels reduces the adhesion of inflammatory cells onto the hydrogel surface and decreases the probability of capsule formation. However, this property also prevents the adsorption of bioactive molecules, such as extracellular matrix (ECM) proteins, which support the growth and function of encapsulated cells [63].

Consequently, this diminishes the viability of encapsulated cells that rely on interactions with the surrounding matrix. Thankfully, functional moieties can be readily integrated into PEG hydrogels through copolymerization. Additionally, the degradability of the hydrogel can be adjusted through the use of degradable or non-degradable crosslinkers (as it was done in this thesis work).
Numerous important studies have clarified the structure-property relationships of PEG-based hydrogels, particularly concerning equilibrium swelling, mechanical characteristics and transport properties [64].

Emerging from these investigations, many PEG-based hydrogel systems have been designed for the controlled delivery of a wide array of biomolecules, spanning from small molecular weight drugs to large biomacromolecules like nucleic acids, peptides, and proteins. Given the diversity in the chemistry and size of the delivered molecules, the design

considerations for controlled release in PEG-based hydrogels can vary significantly across different applications. Nonetheless, the availability and stability of the therapeutics remain two primary concerns when formulating PEG hydrogels for controlled release applications.
To attain the desired therapeutic efficacy in vivo or in vitro, PEG hydrogels must be capable of delivering therapeutics at the appropriate dosage (availability) while preserving molecular bioactivity (stability). The mechanisms governing drug release from PEG hydrogels are based on multiple factors, including: the method of drug loading, the size and molecular properties of the drug and the required dosage and release profile for a specific therapeutic application. In general, the molecular release mechanisms in PEG hydrogels include diffusion-, swelling- and chemically-controlled delivery. One direct approach to modulate molecular release kinetics is by adjusting the gel permeability through tuning the network crosslinking density [60].

2.4.5 PEG Hydrogels applications

Looking at the potential applications of PEG hydrogels, a premise must be made regarding the ECM environment, which the hydrogel needs to emulate to guarantee the same cellular mechanisms as in a biological environment.
Cell migration through extracellular matrices (ECMs) plays a game-change role in various physiological and pathological scenarios, spanning from morphogenesis and regeneration, to tumor invasion and metastasis. The molecular mechanisms governing three-dimensional (3D) migration are intricately complex, involving the coordination of both biochemical and biophysical interactions between cells and the matrix. Given that the ECM often poses a barrier to migration, cells must employ strategies to overcome the biophysical resistance presented by their surrounding matrix [65].

Two primary strategies for single-cell movement, termed proteolytic (or mesenchymal) and non-proteolytic (or amoeboid) migration, have been elucidated for several cell types. It is widely accepted that tumor cells and many stromal cells, such as fibroblasts or endothelial cells, mainly utilize proteolytic strategies for 3D migration [66]. During migration, these cells secrete soluble or cell-surface-associated proteases, including matrix metalloproteinases (MMPs) and serine proteases, which facilitate specific and localized matrix degradation.

On the other hand, studies utilizing protease inhibitor cocktails have demonstrated that migrating leukocytes, such as T lymphocytes and dendritic cells, employ non-proteolytic, path-finding migration strategies to navigate through ECM barriers [67] [68].
In this scenario, 3D migration occurs autonomously of structural matrix remodeling, characterized as an amoeboid process propelled by cell-shape adaptation, brief low-affinity interactions with the environment, propulsive squeezing through preexisting

matrix pores, and elastic deformation of the ECM network. Recent investigations on both neoplastic and non-neoplastic cells are uncovering that the adoption of a specific mode of 3D migration is not inherently restricted to cell types but rather dynamically and reversibly governed by environmental signals [69]. Consequently, cell migration has been extended by a new variable, plasticity in migration mode [70].

PEG hydrogels have been utilized for many different applications, such as for the functional reconnection of severed mammalian spinal cord axons by Shi, Borgens and Blight [71] to reconnect the two segments of completely transected mammalian spinal axons within minutes.
To achieve this, researchers fused completely severed strips of isolated guinea pig thoracic white matter, maintained in vitro within a double sucrose gap recording chamber. The severed segments were aligned, and PEG was applied directly to the region via a micropipette and then promptly removed by aspiration within 2 minutes. Successful fusion was confirmed by the immediate restoration of compound action potentials through the original transection and by observing varying numbers of fused axons with restored anatomical continuity under high-resolution light microscopy. Additionally, the diffusion of intracellular fluorescent dyes through fused axons further supported the conclusion that some severed spinal axons, following PEG-fusion, exhibited both restored anatomical continuity and physiological competency to conduct action potentials [71].

Another example of PEG application for tissue engineering is reported by Burdick's and Anseth's research [72]. PEG hydrogels were explored as encapsulation matrices for osteoblasts to evaluate their potential for promoting bone tissue engineering. Non-adhesive hydrogels were modified with adhesive Arg-Gly-Asp (RGD) peptide sequences to enhance the adhesion, spreading and subsequent cytoskeletal organization of rat calvarial osteoblasts. Upon attachment to hydrogel surfaces, there were notable differences in the density and area of osteoblasts between modified and unmodified hydrogels. A concentration-dependent effect of RGD groups was observed, with higher RGD concentrations correlating with increased osteoblast attachment and spreading, and only the highest peptide density facilitating cytoskeletal organization. The majority of osteoblasts survived the photoencapsulation process when gels were formed with 10% macromer, but there was a decrease in osteoblast viability of 25% and 38% after 1 day of in vitro culture when the macromer concentration was increased to 20 and 30 wt%, respectively. There was no statistically significant difference in cell viability when peptides were incorporated into the network. Finally, mineral deposits were observed in all hydrogels after 4 weeks of in vitro culture, but a notable increase in mineralization was evident upon the introduction of adhesive peptides throughout the network [72].

Another notable application of PEG is in therapeutic vascularization, in a study by A. Edward et al. which remains a significant challenge in regenerative medicine. Whether the objective is to stimulate vascular growth in ischemic tissue or upscale tissue-engineered constructs, the ability to induce the formation of functional, stable vasculature represents a critical challenge. PEG-based bioartificial hydrogel matrices, incorporating protease-degradable sites, cell-adhesion motifs and growth factors, have been engineered to promote vascular growth in vivo.

In comparison to the injection of soluble vascular endothelial growth factor (VEGF), these matrices sustainably delivered VEGF levels in vivo for up to 2 weeks as the matrix degraded. Upon subcutaneous implantation in rats, degradable constructs containing VEGF and arginine-glycine-aspartic acid (RGD) tripeptide induced a significant increase in the number of vessels infiltrating the implant at 2 weeks, with vessel density further escalating at 4 weeks. The enhanced vascularization mechanism is likely driven by cell-demanded release of VEGF, as the hydrogels may substantially degrade within the same timeframe. In a mouse model of hind-limb ischemia, the delivery of these matrices led to a significantly accelerated rate of reperfusion. These findings underscore the potential of engineered bioartificial matrices in promoting vascularization for targeted regenerative therapies [73].

2.5 Boron and its current applications

Within the current research landscape, there is a noticeable lack of studies exploring the application of hydrogels embedding boron sequences for muscle regeneration. Despite the promising implications of this new methodology in the realms of tissue engineering and regenerative medicine, its exploration within existing literature remains notably limited. This pioneering endeavor highlights the absence of prior scrutiny regarding the implementation of these bioactive components for muscle reconstruction.
Taking this unexplored trajectory, this research endeavors to address a significant gap in scientific investigation and contribute to the nascent domain of muscle tissue engineering. Through meticulous experimentation and analysis, it seeks to lay the groundwork for future breakthroughs and therapeutic interventions in muscle regeneration.
In the domain of hydrogel-based muscle reconstruction, Dr.Rico Tortosa and her research team, from the Universitat Politecnica de Valencia, have made groundbreaking investigations into the integration of boron for such objectives. Part of their researches have revolved around the incorporation of RGD-boron and its compounds, revealing the potential of boron-based compounds in the realm of regenerative medicine.

This innovative approach has shed light on the distinctive attributes of boron and its prospective applications in tissue engineering.
Skeletal muscle integrins bind to muscle ECM, which, as already explained before, is mainly composed of members of the laminin family, fibronectin, proteoglycans and the collagen IV family [74].
Going through the constituents of the basement membrane, fibronectin stands out as a singular multifunctional protein. Its levels surge significantly following muscle injury, playing a pivotal role in facilitating the proliferation and differentiation of satellite cells [75] [76].

In addition to integrins, ion channels have a fundamental role in maintaining cell homeostasis by regulating ion fluxes. However, their significance extends beyond mere ion regulation. Ion channels also serve as molecular sensors capable of detecting various stimuli. These channels can perceive force following activation triggered by a range of factors, including ligand binding, membrane stretch, interaction with specific ligands, or alterations in membrane potential. This multifaceted capability underscores the versatility and importance of ion channels in cellular function and signaling pathways, [77] so they can communicate extracellular signals to the cytoplasmic environment [78] and integrins [79].

Skeletal muscle Ion-channels contribute in a very significant way, since extracellular Ca2+, K+ and Cl- play an essential role in muscle cell adhesion, muscle development, migration and fusion [80], even if their particular roles in muscle regeneration are still being discussed and the information available is limited to Ca2+, K+ and Cl- channels [81].
The NaBC1 boron (B) transporter regulates borate homeostasis and functions as an obligated Na+ - coupled borate co-transporter [82]. After NaBC1 is activated, it stimulates intracellular signaling and consequently guarantees vascularization in coordination with growth factor receptors and $\alpha 5\beta 1/\alpha v\beta 3$ integrins [83].
Despite these findings, our understanding of boron homeostasis and its functions within mammalian cells remain limited. To date, only a single study has explored the potential impact of boric acid on muscle differentiation from adipose-derived stem cells. This highlights the necessity for further investigation into the roles of boron in cellular processes and development. [84].
However, boron is a metalloid highly utilized in medicinal chemistry applications[85], and several biomaterial-based approaches use boron as an intrinsic component of the biomaterial platforms for diverse applications [86] [87].

Boron's importance in mammalian cells is well recognized, as it actively participates in various metabolic pathways either independently or in conjunction with other minerals like Ca2+ and Mg2+, along with steroid hormone molecules. This multifaceted involvement underscores the significance of boron in cellular functions and highlights its role as a crucial element in maintaining physiological processes within mammalian organisms [88]. Prior studies have also suggested that boron might play a role in bone mineralization and structure. Moreover, these studies indicate that dietary boron intake could significantly impact calcium (Ca2+) and phosphorus (P) metabolism, particularly under conditions of nutritional stress, such as calcium or phosphorus deficiency. This underscores the potential importance of boron in maintaining skeletal health and highlights its interactions with essential minerals in the body [89].

The approval of a boron-containing peptidic proteasome inhibitor, bortezomib (Velcade), by the U.S. Food and Drug Administration (US FDA) for multiple myeloma and cell mantle cell lymphoma [90], upgraded the area of boron in medicinal chemistry.
In contemporary times, numerous boron-containing molecules are undergoing preclinical and clinical development stages aimed at treating various disease conditions. These conditions span a wide spectrum, including inflammation, diabetes, cancer, and numerous others. This suggests a growing interest in exploring the therapeutic potential of boron-based compounds across diverse medical fields, indicating their promising role in addressing a range of health challenges [91]. In the biomedical field, and specifically of tissue engineering , boron has been utilized for the optimization of biomaterials

particularly in the bioactive glass research area[92] [93], in which new bioactive glasses based on borate and borosilicate compositions have demonstrated to posses the capacities to improve new bone tissue formation when compared with silicate bioactive glass.

Indeed, borate-based bioactive glasses exhibit controllable degradation rates, offering better conditions for scaffold materials utilized in both hard and soft tissue regeneration. This feature makes them particularly valuable in tissue engineering applications, where the controlled degradation of scaffolds is fundamental for promoting appropriate tissue growth and integration. By exploiting borate-based bioactive glasses, researchers can tailor scaffold properties to suit specific tissue regeneration needs, thereby advancing the field of regenerative medicine [94].

Boron has also been used in the synthesis of biodegradable polymers [95]. In the realm of muscle tissue regeneration, a recent study has shed light on the dose-dependent activity of boron in the myogenic differentiation of human adipose-derived stem cells. However, despite this advancement, the biochemical mechanism underlying boron's action, remains incompletely understood. Until recently, it was commonly believed that boron and borates entered cells through passive diffusion across the cell membrane [96] [97].

Considering the vital role of borate as a micronutrient in plants and animals and the uniqueness of boron as a novel challenging element for tissue engineering, the following study by Dr. Rico Tortosa et al. [98] was set out to investigate whether boron promoted cell differentiation per se when released from a poly(l-lactic acid) (PLLA)-based system.
Although the initial cell density was consistent across all substrates, the final cell density at the conclusion of the culture varied due to the influence of intrinsic material properties on cell behavior, particularly determined by borax-d content. It's crucial to highlight that the ultimate cell count does not directly correlate with the degree of myogenic differentiation. This observation challenges the notion that differentiation is solely a consequence of cell density, as previously suggested [99].
Additionally, the number of cells observed on the PLLA-borax-d 5% and PLLA-borax-d 2% samples was slightly lower compared to the collagen I control. This discrepancy suggests the potential of borax-d to induce fusion, leading to the formation of multinucleated myotubes. Myotube formation under various conditions was assessed through immunostaining of sarcomeric α-actinin and visualized using laser scanning confocal microscopy. Upon differentiation induction, PLLA-borax-d 2% and 5% substrates exhibited distinct accumulation of sarcomeric α-actinin in a punctate pattern along the longitudinal axis of the myotube, closely associated with actin filaments.

This finding further supports the notion that borax-d enhances skeletal myogenesis by modulating the developmental program directing myoblasts towards muscle fiber differentiation. Calcium signaling is integral to the differentiation of numerous cell types, including skeletal muscle cells [95]. However, its mechanisms remain poorly understood due to the diverse effects of calcium on various metabolic pathways. The lack of an observable effect of extracellular calcium on cell differentiation on borax-d-loaded substrates may seem contradictory if we solely consider calcium transport through plasma membrane channels: one might expect higher levels of cell differentiation with increased extracellular calcium. However, it's important to consider that an elevation in intracellular calcium concentration can also result from calcium release from intracellular stores regulated by second messengers or calcium itself [98].

An alternative explanation for the effects of calcium on borax-d-loaded materials lies in the chelation of calcium ions by borax-d. Borax decahydrate is commonly used for water softening (sequestration of calcium ions) in detergents. In this scenario, the addition of extracellular calcium might sequester borax-d released from PLLA, preventing its association and active transport by the Na+ - coupled borate cotransporter, NaBC1, thereby impeding calcium entry through the cell membrane. The formation of the borate anion-Ca2+ complex would lead to reduced availability of calcium ions, resulting in effects similar to those of EGTA or verapamil chemicals. This chelating effect is amplified with higher concentrations of extracellular borax-d [98].

Fully developed vascular networks are vital for the proper functioning of cells and tissues. These networks consist of hierarchical blood vessels that permeate throughout, delivering oxygen and nutrients while eliminating toxic metabolites. Beyond facilitating various essential cellular functions, vascularization is a fundamental process implicated in inflammation, tumor progression, and metastasis. This process is regulated by vascular endothelial growth factor (VEGF), which interacts with its receptor (VEGFR) to orchestrate vascular development and function [100].

Contemporary approaches to improve vascularization primarily involve the utilization of growth factors (GFs). These strategies range from straightforward delivery systems to intricately engineered synergistic bioactive materials [101] [102]. Despite concerted efforts, strategies relying on growth factor (GF) delivery often necessitate the use of high concentrations to offset their low stability and restricted mode of action.

Angiogenesis, the formation of new blood vessels, is intricately regulated by the dynamic interplay among growth factors, the extracellular matrix (ECM), and integrins [103]. Integrins, as already mentioned above, represent a family of transmembrane glycoproteins crucial for cellular function. Upon binding to a diverse array of extra-

cellular matrix (ECM) components like fibronectin (FN), collagen, laminin, fibrinogen (FG), or other surface receptors, integrins become activated. Serving as mechanosensors, they play a pivotal role in mediating both mechanical forces and biochemical signals. This regulation of multiple cellular events underscores the significance of integrins in cellular physiology and signaling pathways [104]. The relevance of the interactions between integrins and GF has been extremely demonstrated as well as the interplay between GF receptors, integrins, and other transmembrane proteins [105] [106] [107]. Ion channels, integral membrane proteins, govern the flow of ions across cell membranes. In addition to their role in regulating cell homeostasis, they also serve as mechanosensors, transmitting extracellular signals to both the cytoplasmic environment and integrins [108].

This multifaceted functionality underscores the importance of ion channels in cellular communication and signaling pathways [109] [110]. Recently, the role of certain calcium and potassium channels has emerged as potential therapeutic targets for cancer treatment, primarily because of their significance in tumor vascularization. These channels have garnered attention for their involvement in the formation of blood vessels within tumors, a process crucial for tumor growth and metastasis. Targeting these channels holds promise for disrupting tumor vascularization and inhibiting tumor progression, making them attractive candidates for cancer therapy [111].

Chapter 3

Materials and methods

3.1 Physico-chemical characterization of the PEG-Hydrogels

3.1.1 Synthesis

Figure 3.1: Utilized liquid mixture for the hydrogels before their crosslinking

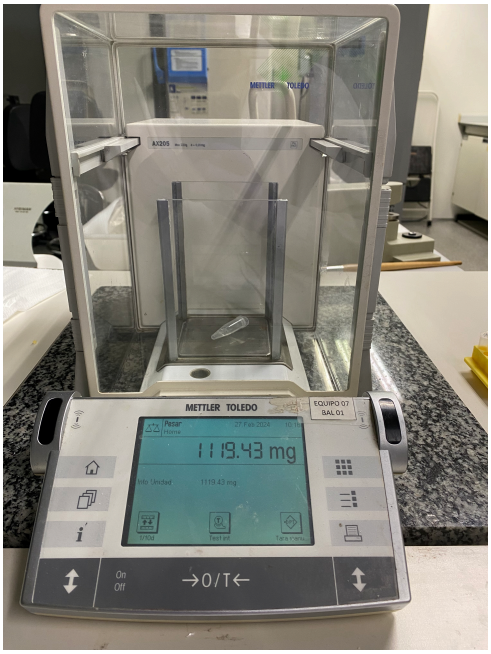

Figure 3.2: AX205 DeltaRange - Mettler Toledo balance for the weights measurements

In this project 3D hydrogel systems were developed based on polyethylene glycol (PEG), degradable by proteases and simultaneously presenting boron compounds and cell adhesion domains.
The degradability of the hydrogels was controlled by combining the PEG-4MAL (PEG with 4 terminal maleimide groups and ratios of non-degradable/degradable crosslinkers like: VPM (a peptidic short crosslinker easily cleavable by the metalloprotease (MMPs)

composed of Valine, Proline and Methionine) and PEG-diSH (polyethylene glycol dithiolate, with two thiol groups). As it can be deduced by the name, crosslinkers conduct and manage the crosslinking phase of the hydrogel, which consists in the passage from liquid to gel through different chemical reactions.
These crosslinkers were used at the same ratio (50/50) so that the hydrogel had a degradation rate of the 50%.
For the following assays different samples were made: controls (made just of PEG), PEG with 2mM RGD sequence, PEG with 6mM RGD-Boron, and PEG with 6nM RGD-Bortezomib.

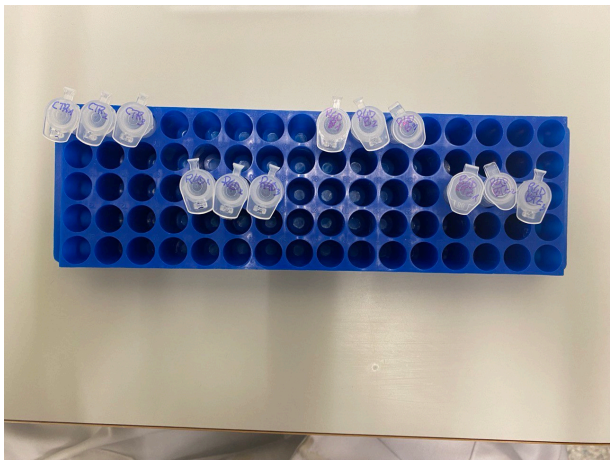

Figure 3.3: Hydrogels utilized in the following experiments: three per condition.

The synthesis procedure was based on the following protocol.
First, the correct quantities of PEGMAL, VPM, and PEG-diSH were carefully weighed with the AX205 DeltaRange - Mettler Toledo balance (Figure 3.2), ensuring accuracy, as illustrated in Figure 3.3 below. Once the appropriate amounts had been measured, they were diluted in the corresponding volumes of PBS +/+ buffer solution, with the volumes specified in Figure 3.4 below. This step was crucial for achieving the proper concentration and consistency of the solution.
Next, 1 L of each of RGD, RGD-B and RGD-BTZ, was added to the PEG-MAL solution. These components were already in liquid form, which simplified their integration into the mixture.
Following this addition, the combined solution was incubated for 30 minutes at 37°C. This incubation period allowed for adequate mixing and reaction among the components.
While the PEGMAL solution was incubating, the crosslinker mixture was prepared by thoroughly mixing the two crosslinker compounds together.
Once they were well-mixed, 10 μL of the crosslinker mix was dispensed into each prepared sample, as demonstrated in Figure 3.5 below. This precise addition was essential for the subsequent crosslinking process.
Finally, the samples were left for 60 minutes at 37°C in the incubator. This step facilitated the crosslinking process, ensuring that the components properly bounded together to form

the desired hydrogel structure. The controlled temperature and time were critical factors in achieving optimal crosslinking efficiency and stability of the final product.
This protocol followed these corresponding quantities:

WEIGHTS					
	0mM RGD (3 wells)	**2mM RGD (3 wells)**	**6nM RGD-B (3 wells)**	**6nM RGD-BTZ (3 wells)**	
PEGMAL	**7.5 mg**	7.5 mg	7.5 mg	7.5 mg	**→ TOT: 7.5mg x 3 = 22.5 mg**
RGD	/	/	/	/	
RGD-B	/	/	/	/	
RGD-BTZ	/	/	/	/	
VPM					**→ TOT : 2.54 mg**
PEG-diSH					**→ TOT: 5.1 mg**

Figure 3.4: Utilized weights for the synthesis of the different hydrogels (three for each condition)

VOLUMES of PBS +/+					
	0mM RGD (3 wells)	**2mM RGD (3 wells)**	**6nM RGD-B (3 wells)**	**6nM RGD-BTZ (3 wells)**	
PEGMAL	40 x 3 = 120 µl	39 µl	39 µl	39 µl	In one eppendorff→ **TOT: 39 µl x 9 wells = 351 µl**
RGD	/	/	/	/	
RGD-B	/	/	/	/	
RGD-BTZ	/	/	/	/	
VPM					In one eppendorff→ TOT: 5µl x 12 = 60 µl
PEG-diSH					In one eppendorff → TOT: 5µl x 12 = 60 µl

VOLUMES IN EACH WELL					
	0mM RGD (3 wells)	**2mM RGD (3 wells)**	**6nM RGD-B (3 wells)**	**6nM RGD-BTZ (3 wells)**	
PEGMAL	40 µl	39 µl	39 µl	39 µl	In one eppendorff → **TOT: 39 µl x 9 wells = 351 µl**
RGD	/	1 µl	/	/	
RGD-B	/	/	1 µl	/	
RGD-BTZ	/	/	/	1 µl	
VPM	5 µl	5 µl	5 µl	5 µl	
PEG-diSH	5 µl	5 µl	5 µl	5 µl	

Figure 3.5: Utilized volumes of PBS+/+ for dilution (above) and to put in each well for the construction of the different samples (three each)

3.1.2 Swelling

The swelling assay had the main goal to calculate the percentage of swelling rate (Q%) by submerging three hydrogels for each type of condition (CTRLS, RGD, RGD-B and RGD-BTZ) in 1 ml of water MilliQ and letting the hydrogels absorb it for: 5, 10, 30, 60, 120, 240, 1080 and 1440 min.
We measured their weigh at the beginning and, after each of these time periods, it was measured again.
The swelling rate was then calculated with the following formula (Equation 1), based on the initial weigh and the final weigh obtained after each time period.

$$Q(\%) = \left(\frac{w_f - w_0}{w_0} \times 100 \right)$$

Equation 1: Calculation of the swelling percentage rate where wf is the final weigh, while w0 is the initial one

3.1.3 Degradation

Hydrogels were synthetized as mentioned before creating the same four conditions (CTRLS, RGD, RGD-B and RGD-BTZ) and then soaked in 200 μL of PBS-/- and 1 ml of 1 mg/ml of collagenase. This enzyme specifically recognises the VPM peptide within the material, which is cut by the collagenase by breaking its peptide bonds.
The degradation of the VPM crosslinker leads to the breakdown of the hydrogel's lattice structure, causing it to lose weight. The hydrogels were weighted before starting the assay and then after 1, 2, 4, 8, 24, 48, 72 and 144 hours. After each time point, fresh collagenase solution was added for the following measurement.
Finally, it was possible to calculate the degradation rate (D%) with the following formula (Equation 2), based, as the one before, on the initial and final weight:

$$D(\%) = \left(\frac{w_0 - w_f}{w_0} \times 100 \right)$$

Equation 2: Calculation of the degradation percentage rate where w0 is the initial weight and wf is the final one.

3.1.4 Rheology

For the rheometer assay we produced six samples for each condition (CTRLS of just PEG, PEG-RGD, PEG-RGD-B and PEG-RGD-BTZ) following the same procedure of synthesis, but with the new corresponding quantities (which simply corresponded to the double of the weighs and of the volumes for diluition of PBS+/+ utilized in the preceeding assays). After incubation in PBS -/- overnight to ensure total hydratation, we procedeed with the rheological analysis by using the Discovery HR-2 hybrid rheometer inserting a stem of 8mm. Everything had to be stable at a temperature of 37°C. We decreased the gap between the stem and the sample till we reached an axial force of approximately 0.06N. We then proceeded with two different analysis:

- The strain sweep: this type of test involved applying to our samples different strain (deformation) amplitudes, while the frequency remains constant. During the test, the amplitude of the strain is varied and the material's response is monitored, observing how the stress varies as a function of strain. For this test, in the oscillation parameters, it was imposed a constant frequency sweep of 1 Hz and a strain sweep between 0.01%-1%.

- The frequency sweep: in this analysis the frequency of oscillation varies and it is observed how the strain changes as a function of the applied frequency. For this analysis it was established an angular frequency between 0.01-10 Hz, with a constant strain of 1%.

These types of test are useful to determine the strain range and to assess the viscoelasticity of the material.

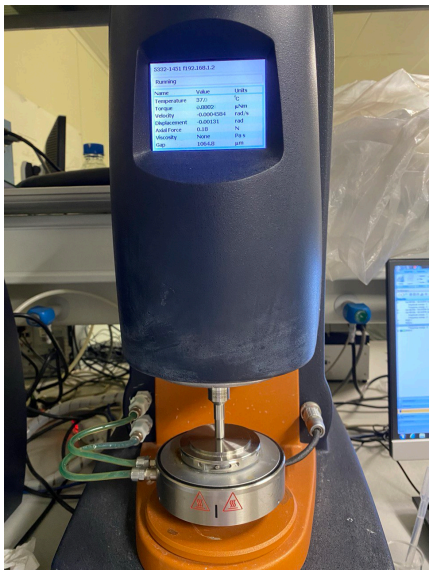

Figure 3.8: Discovery HR-2 hybrid rheometer during the test

Figure 3.9: Zoom of the same test from the previous image

3.2 In vitro assays

3.2.1 Cell culture

The preparation of the cells followed the protocol that is reported below.
In the cabin, various preparations were made, such as:

- Normal colture medium: which was composed of 45 ml of DMEM HIGH P/S and 5 ml of FBS
- Trypsin, a proteolytic enzyme necessary for the cell detachment
- DPBS -/-
- Two flasks already prepared containing human fibroblasts corresponding to two different cell lines: a wild type (WT) and a mutant type (FN-/FN-).
This last one in fact did not produce fibronectin. These cells were immerged in 10 ml of medium (FBS 10% and DMEM HIGH P/S 90%).

The next step involved extracting the normal medium from the two cell flasks. Following this, the cells were washed with DPBS -/- (5ml), ensuring meticulous washing along the flask walls and surrounding areas to prevent any remaining culture medium from inactivating the trypsin and its action.
After removing the DPBS -/-, 3ml of trypsin were added to undermine cell adhesion. The cells were then incubated for 5 minutes at 37°C in the incubator.
Subsequently, cell adhesion was observed under the Nikon DS-Fi1 Microscope.
To deactivate the trypsin action, 3 ml of normal cell culture medium was added. Any remaining adhered cells were detached using an electronic pipette, moving the content up and down through it.
The contents of the two flasks were then transferred into 15 ml tubes and centrifuged at 1000 rpm for 5 minutes.
The supernatant was then discarded, and the cell pellet was resuspended in normal medium.
Finally, the cells were counted using a Neubauer's Chamber, and the cells that weren't necessary for this particular assay were seeded into a new flask for further experimentation.

3.2.2 MTS assay

To verify the cytotoxicity of the material towards cells, it was performed a viability assay which relies on the reduction of the MTS reagent [3-(4,5-dimethylthiazol-2-yl)-5-(3-carboxymethoxyphenyl)-2-(4-sulphophenyl)-2H-tetrazolium] into a coloured formazan compound due to NADPH (Nicotinamide Adenine Dinucleotide Phospate), and is dependent of the dehydrogenase enzymes in cells metabolically active.
The absorbance of the formazan dye can be measured at a specific wavelength of 490 nm using a spectrophotometer.
We prepared six hydrogels for each condition (CTRLS of PEG, PEG-RGD, PEG-RGD-B and PEG-RGD-BTZ). After the preparation of the cells, it was utilized a Neubauer chamber to count the necessary volumes of cells to put in two phials (one for the WT and one for the FN-/FN-). Considering that it was necessary a quantity of 40000 cells for each sample, it was calculated that the correct volumes of cells to extract were 0.176 ml in total for the WT and 0.150 ml in total for the FN-/FN-.
These quantities were added respectively to 17.824 ml and 17.850 ml of normal medium to obtain 18 ml of the total composite for each line of cells (considering 500 μL for each of the 36 samples for each line of cells). So, 500 μL were extracted from the previous compound and put in the 36 samples for each line of cells and, after, the corresponding hydrogels were positioned in the wells.

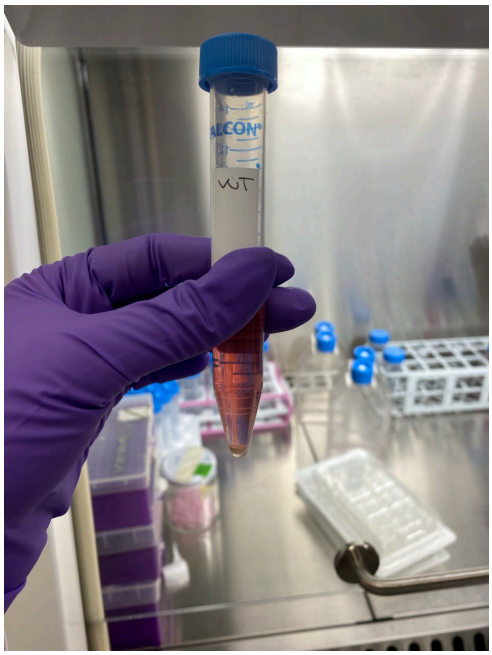

Figure 3.10: Tube containing wild type cells (WT) and normal medium after the centrifuge

We then waited 24 hours and proceeded as follows.
We firstly began by heating the phenol red-free medium and the MTS, a crucial preparatory step to facilitate subsequent reactions.
Following this, we meticulously prepared the phenol red-free medium and MTS composite. This involved precise measurements, as we combined 12960 µL (36 samples x 360 µL/well) of phenol red-free medium with 1440 µL (36 samples x 40 µL/well) of MTS, resulting in a total compound volume of 14400 µL.
Moving forward, we initiated the cell death control phase by introducing 500 µL of Ethanol 70% into each of the six wells designated for the dead control on the 24-hour plate. With this control in place, we proceeded to extract the hydrogels from the wells, preparing them for further observations.
Subsequently, we extracted the hydrogels and then we allowed the samples to incubate for 10 minutes while examining them under the Nikon DS-Fi1 Microscope. This observation phase was crucial, as we carefully checked all conditions across the two 24-hour plates, capturing three photos for each condition to document our findings.

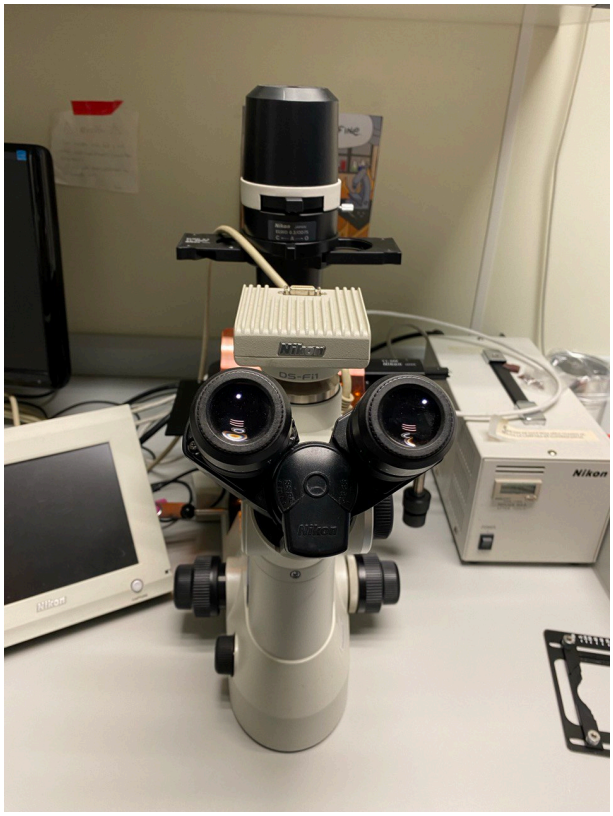

Figure 3.11: Nikon DS-Fi1 Microscope

After the extraction of the medium, we then added 400 µL of the phenol red-free medium + MTS composite into each well of the two plates, ensuring uniformity across our samples.

Once again, we allowed the composite to incubate, this time for a duration of one hour at 37°C, providing optimal conditions for the reactions to occur.
Subsequently, we transferred cells from the two 24-hour plates to two 96-well plates, extracting 100 µL of the composite + cells from each well of the 24-hour plates to populate the 96-well plates.
Finally, we utilized the Victor spectrophotometer, employing the A490 program with a 0.1-second duration, to measure the absorbance of our samples. This critical step allowed us to quantitatively assess the outcomes of our experiment, providing valuable data for analysis and interpretation.
Once calibrated, the instrument is, in fact, set to measure light at a specific wavelength of 490 nm. This is the wavelength at which the formazan (obtained from the reduction of the MTS) is expected to absorb light. The samples are indeed exposed to light at 490 nm emitted by the light source of the spectrophotometer. The amount of light absorbed by the sample at 490 nm is detected by a photosensitive detector in the instrument. This detector converts the absorbed light into an electrical signal that is recorded by the spectrophotometer. The electrical signal produced by the detector is analysed by the instrument to determine the absorbance of the sample at 490 nm. The absorbance is proportional to the concentration of formazan in the samples that absorbs light at that specific wavelength. For this reason, the more absorbance is detected, the more NADPH enzyme was present to carry out the reduction from MTS to formazan. Consequently, this represents a high presence of alive cells.
The same protocol was then followed for the other plates after 72h to verify the viability of cells after a different and longer time period.

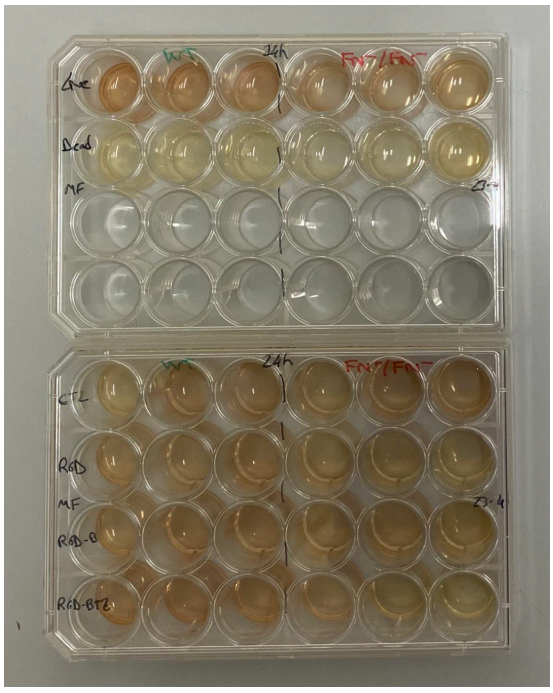

Figure 3.12: MTS samples before the analysis with the spectrophotometer (above: the live and death control for the two cell lines, below: the four conditions for the experiment.

Figure 3.13: PERKIN ELMER Victor X3 Multilabel Reader Board Spectrophotometer

3.3 CAM assay

The CAM assay was conducted to evaluate the pro-angiogenesis effect of our hydrogels in an in vivo model.
Twenty fertilized chicken eggs were utilized at day seven post-fertilisation from "Productos Florida S.A." farm (Villarreal, Spain) and were kept in an incubator at 37°C.
On day eight after fertilization, eggs were candled to detect and mark the air chamber of the chick embryo and the eggshell was cut on top of the air chamber to expose the CAM (Chorioallantoid membrane). Once the membrane was exposed, hydrogels were implanted carefully on top of the chorioallantoic membranes and then, the shell windows were sealed with parafilm and the eggs were placed back in the incubator.
Four replicates per condition were used:

- PBS-/-: just the embryos without any hydrogel, but just PBS -/- to highlight the vascularisation in the following analysis;
- Controls with just PEG hydrogels;
- PEG-RGD hydrogels;
- PEG-RGD-B hydrogels;
- PEG-RGD-BTZ hydrogels.

96 hours after implantation, incubating at 37°C, the sealings were removed and the vasculature was imaged using a stereomicroscope, the Leica MZ APO X16 magnification. We took about six photos for each sample of each condition with the optical microscope (so for a total of approximately 120 photos).

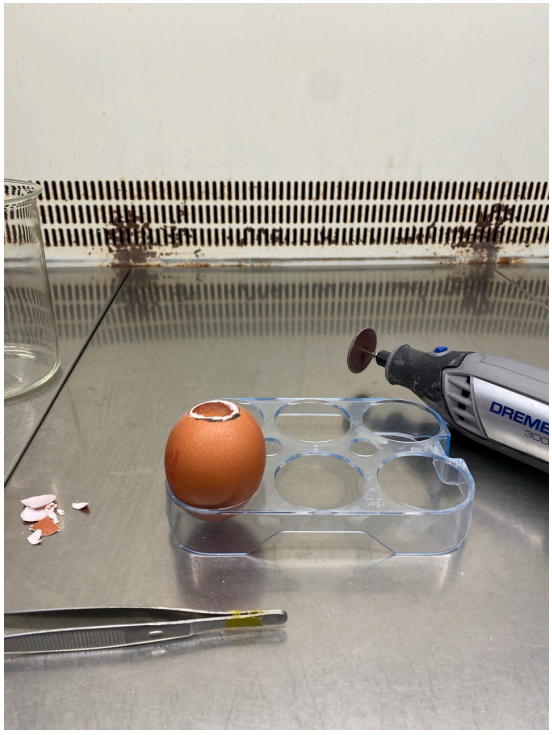

Figure 3.14: Cut of the air chamber through a milling cutter and the help of a pair of tweezers.

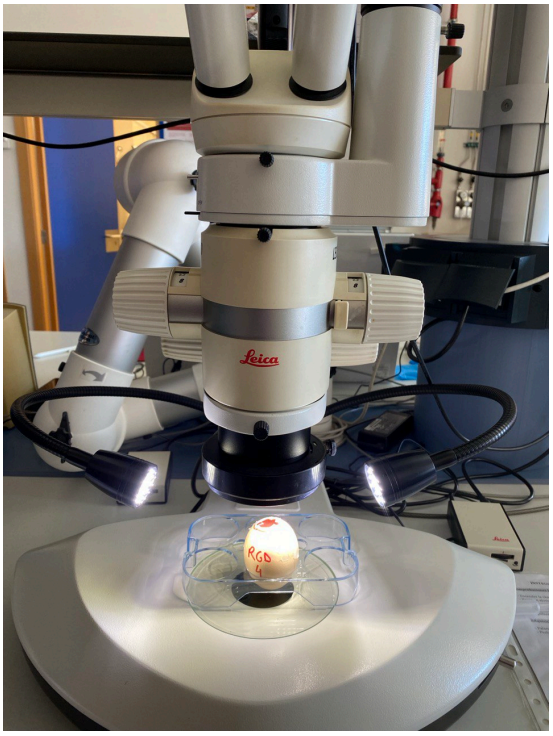

Figure 3.15: Leica MZ APO X16 magnification microscope utilized for the verification of angiogenesis in the embryos.

Blood vessels were marked manually with Image J software, tracing a line on top of each vessel that could be found in the images taken previously with the microscope.

Figure 3.16: ImageJ software

This process resulted in producing different masks for each image which were used to quantify, afterwards through the AngioTool software, the vessels area, vessel density, total number of junctions, branching index, total vessel length, average vessel length, total number of end points and lacunarity.

Figure 3.17: Highlighted blood vessels with the Image J software

In this last analysis with the AngioTool software, we imposed a vessel diameter and intensity between 6 and 19, as it can be seen in the Figure 3.18 . Here is the representation of the Angiotools software with the correct parameters described above, while analyzing a sample.

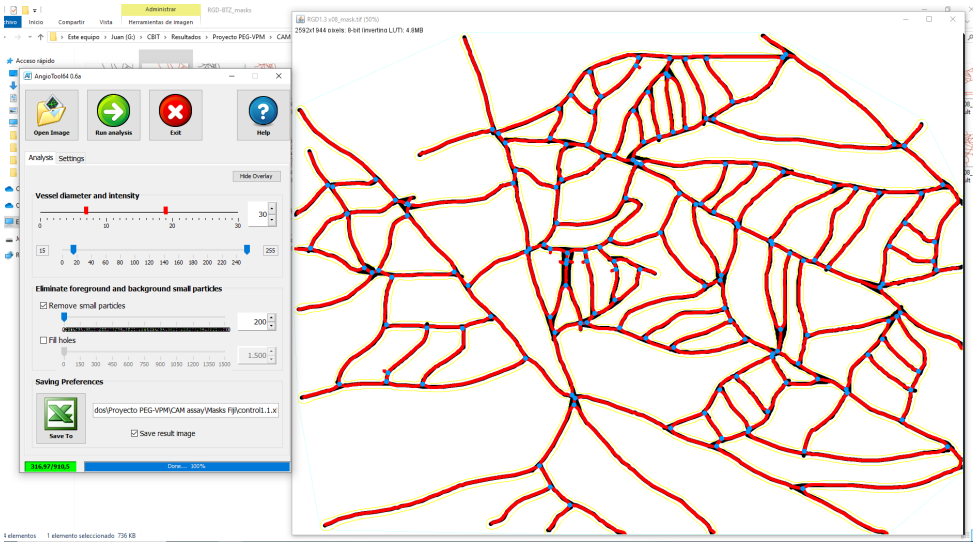

Figure 3.18: AngioTool software utilized to highlight the characteristics of the vessels and obtain the data

Here below is reported a specific table (Table 3.1) that summarizes all the main analyzed characteristics of the vessels through the AngioTools software and their specific definition and meaning.

Parameter	Definition
Vessels area	Area occupied by vessels.
Vessel density	Percentage of area occupied by the vessels in a particular area.
Total number of junctions	Total number of points in which two or more vessels meet.
Branching index	Number of vessels junctions normalized per unit area.
Total vessels length	Sum of Euclidean distances between the pixels of all the vessels.
Average vessels length	Mean length of all the vessels.
Total number of end points	Number of points in which a vessel ends, so of open ended segments.
Lacunarity	Degree of inhomogeneity of the sizes of the gaps/lacunae surrounded by vessels

Table 3.1: Summary of angiogenesis-related parameters analyzed with AngioTool software

3.3.1 Statistical analysis

For the statistical analysis, data were analyzed using GraphPad Prism software where normality tests were performed to determine whether to select parametric or non-parametric tests. Then appropriate one-way ANOVA for multiple comparisons was used. Statistical differences were defined by p values and confidence intervals were indicated with asterisks (*). In particular they represent a p value respectively: * ≤ 0.05; ** ≤ 0.01; *** ≤ 0.001; **** ≤ 0.0001 (see paragraph of Results - CAM assay).

Chapter 4

Results and discussion

4.1 Physico-chemical characterization of the PEG-Hydrogels

Hydrogels, a class of versatile biomaterials, have garnered significant attention in biomedical engineering due to their tunable properties and wide range of applications in drug delivery, tissue engineering and regenerative medicine. Polyethylene glycol (PEG)-based hydrogels, in particular, stand out for some main characteristics because they offer several advantages in biomedical applications, such as:

1. Biocompatibility: PEG is non-toxic and non-immunogenic, reducing the risk of adverse reactions when used in vivo.

2. Customizable Properties: The mechanical properties, degradability, and bioactivity of PEG hydrogels can be easily tuned by modifying the PEG molecular weight, cross-linking density and functionalization with bioactive molecules.

3. Controlled Drug Release: PEG hydrogels provide a platform for the controlled release of drugs, ensuring a sustained therapeutic effect and reducing the frequency of drug administration.

4. Enhanced Cellular Interactions: Functionalization with peptides like RGD enhances cell-material interactions, promoting tissue integration and healing [60].

In this research project, PEG hydrogels were formulated using 4-armed PEGs with maleimide-terminal groups (PEG-4MAL). The matrices were then functionalized with commercial RGD peptides, a three amino acids sequence (Arginine-Glycine-Aspartic acid) which is found in many proteins (such as fibronectin) of the extracellular matrix and plays a crucial role in cell interaction with their surrounding environment, like cell adhesion (see Introduction paragraph).
This sequence was conjungated to the hydrogels by PEGylation reactions (so through a covalent bond). This process not only ensures the stable incorporation of bioactive cues

but also maintains the mechanical integrity of the hydrogel.
The RGD adhesive sequence promotes cell adhesion, proliferation and differentiation by interacting with cell surface integrins (binding-integrins). This interaction is critical for various cellular processes, including migration and signaling, which are essential for tissue regeneration and repair.
The hydrogels were also simultaneously loaded with boron compounds such as Bortezomib: an antineoplastic drug used in the treatment of malignant tumors. It works, through its boron component, by inhibiting the proteasome, an enzymatic complex inside cells involved in protein degradation. This drug interferes with the cellular process controlling the growth and survival of tumor cells, thereby helping to slow down cancer progression.
The main reason for the introduction of boron is the activation of the boron transporter NaBC1, which, creating a functional cluster with the binding-integrins (activated by the RGD sequence) introduced simultaneously with the boron, guarantees cellular adhesion, proliferation, vitality and consequent possible differentiation to muscular cells.

4.1.1 Swelling

The swelling rate is a fundamental parameter to deepen the hydrogel network structure as well as on how the distance between cross-linking affects the structure [112].
Here following, in Figure 4.1, are all the weights that were obtained (table above) and the average of the weights for each condition (table below).

		Time (min)							
% swelling	Replicate	5	10	30	60	120	240	960	1440
Control	1	128,19	222,30	234,61	269,55	299,53	326,87	343,80	327,41
	2	115,03	122,40	210,27	268,78	316,08	371,43	437,71	627,08
	3	104,33	174,63	224,30	250,49	279,32	326,35	394,04	392,48
RGD	1	109,56	189,96	296,45	348,44	387,02	416,29	451,92	440,20
	2	63,53	102,46	155,62	208,19	241,39	302,22	374,98	459,47
	3	71,47	105,23	156,59	219,03	259,10	311,86	374,98	425,38
RGD-B	1	102,95	154,43	185,91	227,67	290,03	351,07	416,12	448,68
	2	197,68	226,71	285,02	305,65	341,59	370,24	401,30	397,15
	3	90,41	166,33	229,65	253,48	278,25	308,42	360,43	328,94
RGD-BTZ	1	126,12	193,68	244,17	281,18	302,77	338,29	370,33	358,30
	2	199,40	255,52	294,03	328,10	357,33	382,94	389,39	388,48
	3	130,20	205,98	291,49	324,94	346,05	371,26	420,98	397,73

	Time (min)							
% swelling	5	10	30	60	120	240	1080	1440
Control	115,85	173,11	223,06	262,94	298,31	341,55	391,85	448,99
RGD	81,52	132,55	202,89	258,55	295,84	343,46	400,63	441,68
RGD-B	130,35	182,49	233,53	262,27	303,29	343,24	392,62	391,59
RGD-BTZ	151,91	218,39	276,56	311,41	335,38	364,16	393,56	381,50

Figure 4.1: Table above: the obtained data of the three samples for each type, after the weigh. Table below: the calculated average of the % of swelling for each type of sample.

From these weights, it was calculated the swelling percentage rate of each condition with the formula reported in Materials and Methods.
The representative graphics of these results are reported here below, reporting a hyperbolic trend of all our samples, independently from their condition, till the 240 minutes, while and after being immerged in MilliQ water.
After that time period a plateau is visible till the end of the experiment, confirming a stabilization in the structure of our material.
In general, longer cross-linkers (PEG-diSH) will restrain less the swelling capacity of the hydrogels in comparison to shorter chains (VPM). For this reason, degradable hydrogels (PEG-50%) would be expected to swell less than the PEG-0%, as it corresponded in this case comparing the results from the Oliver-Cervell'o's study that utilized a very similar hydrogel but with different proportions of crosslinkers (and so with different degradability and physico-chemical characteristics) [112].

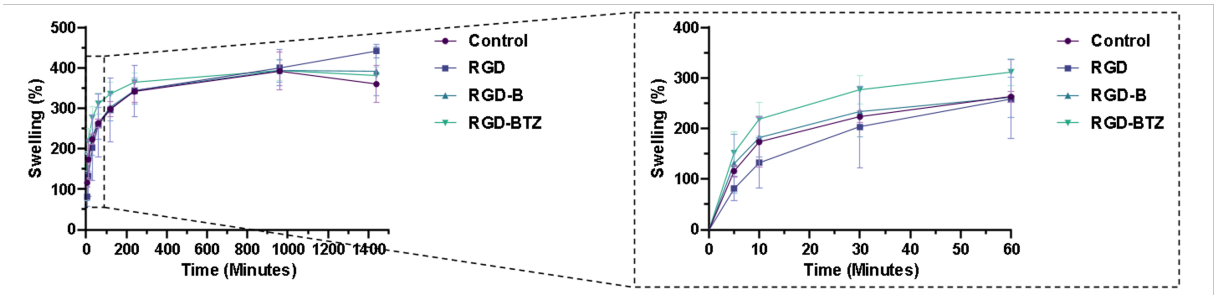

Figure 4.2: On the left: the general trend of the samples when immerged in MilliQ water after different time periods. On the right: a zoom of the first figure representing the analysis and its results from 0 to 60 minutes.

The comparison with the study by Oliver-Cervell'o [112], which utilized a similar hydrogel system with different proportions of cross-linkers, further supports these findings. Their research also reported differences in swelling behavior based on the cross-linker length and concentration, which influenced the hydrogel's degradability and physico-chemical properties.

In summary, the hyperbolic swelling trend, followed by a stabilization phase, underscores the predictable and controllable nature of hydrogel swelling behavior. Longer cross-linkers like PEG-diSH result in hydrogels with higher swelling capacities, while shorter cross-linkers such as VPM limit expansion. Degradable hydrogels, with their denser network, exhibit less swelling compared to non-degradable ones, confirming the relationship between cross-linker length, degradability and swelling capacity.
These insights are critical for designing hydrogels tailored for specific biomedical applications.
In tissue engineering, understanding the swelling properties helps in creating scaffolds that provide adequate support and space for cell growth.

4.1.2 Degradation

It is preferable to have an injectable hydrogel which favours cell adhesion and differentiation and, once the tissue is regenerating, it can dissolve. For this reason, for the beginning of this study, we created a 50% degradable hydrogels (as described before in the Materials and Methods paragraph) and, to verify its degradation characteristics, we utilized samples soaked in collagenase at different times of immersion. Here following are the weighs obtained after different time periods.

		Time (h)							
% mass loss	Replicate	1	2	4	8	24	48	72	144
Control	1	7,58	12,67	15,25	24,52	33,85	38,84	45,65	46,81
	2	9,00	12,84	14,19	23,18	33,29	40,89	48,11	48,63
	3	8,05	10,94	12,68	21,87	35,01	38,35	45,79	46,06
RGD	1	7,75	10,60	12,90	23,55	34,71	42,20	49,02	50,10
	2	7,88	12,05	13,59	24,18	37,89	41,40	46,80	49,61
	3	6,04	11,94	11,96	23,34	35,83	42,58	50,03	51,66
RGD-B	1	8,45	14,11	15,97	20,97	31,52	37,03	51,08	53,04
	2	9,28	13,05	15,36	22,33	33,84	37,76	49,19	50,14
	3	8,77	12,53	14,09	21,90	35,74	41,28	50,46	52,42
RGD-BTZ	1	8,31	11,01	13,13	26,68	35,88	43,64	48,10	48,57
	2	8,38	9,62	12,81	25,11	36,74	41,11	48,99	51,49
	3	9,65	11,57	13,04	27,69	34,68	44,16	49,25	49,80

	Time (h)							
% mass loss	1	2	4	8	24	48	72	144
Control	-8,21	-12,15	-14,04	-23,19	-34,05	-39,36	-46,52	-47,17
RGD	-7,22	-11,53	-12,82	-23,69	-36,14	-42,06	-48,62	-50,46
RGD-B	-8,84	-13,23	-15,14	-21,73	-33,70	-38,69	-50,24	-51,87
RGD-BTZ	-8,78	-10,73	-12,99	-26,49	-35,77	-42,97	-48,78	-49,95

Figure 4.3: Table above: the obtained data of the three samples for each type, after the weigh. Table below: the calculated average of the % of degradation for each type of sample.

The representative graphics of the degradation percentage rate of the samples are reported below, displaying a descending hyperbolic trend indicative of the degradation induced by the introduction of VPM (Valine-Proline-Methionine). Initially, the degradation rate is rapid, suggesting that the VPM significantly accelerates the breakdown of the PEG hydrogels. This quick degradation phase is crucial for applications where a rapid release of encapsulated agents or the timely resorption of the material is desired.

After the initial phase, the trend reaches a stabilization point around the 72-hour mark, which corresponds to the effective 50% degradation rate of our PEG hydrogels. This plateau signifies that half of the hydrogel matrix was degraded within this timeframe, primarily due to the MMPs enzymatic activity targeting the VPM sequences.
This consistent degradation pattern was observed across all conditions tested, indicating that the degradation process is reliable and reproducible.

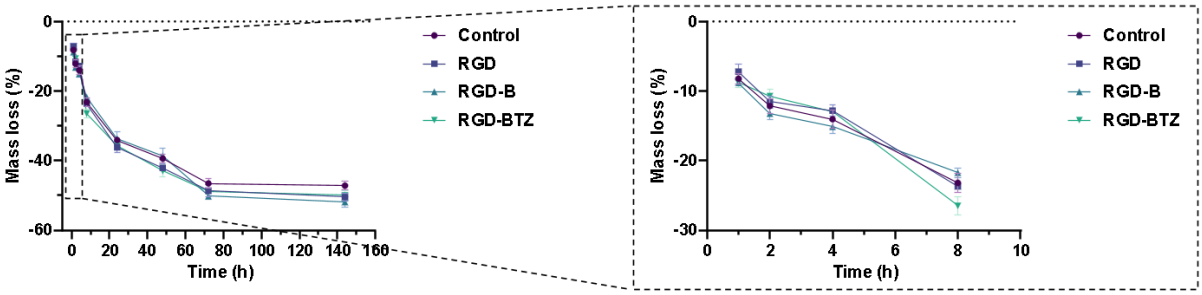

Figure 4.4: On the left: the general trend of the samples at different time periods in collagenase. On the right: a zoom of the first figure which highlights the trend between 0 and 8 hours.

The degradation rate is critical for ensuring that the hydrogel performs its intended function before being safely re-absorbed by the body.

To validate our findings, we referenced the study by Oliver-Cervell'o [112], which provided similar results and reinforced our observations. Their work demonstrated a descending hyperbolic degradation trend too, with a stabilization occurring after a similar period, thus corroborating the effectiveness and consistency of using crosslinkers to control the degradation of PEG hydrogels. In tissue engineering, the gradual degradation of the scaffold provides sufficient support for cell growth and tissue formation before the scaffold is fully resorbed.

Furthermore, the uniform degradation characteristics observed across different samples highlight the robustness of the hydrogel formulation. This consistency is essential for clinical applications, where reproducibility and reliability are paramount. By fine-tuning the composition and cross-linking density of the hydrogels, it is possible to achieve specific degradation profiles tailored to the needs of different medical treatments.

4.2 Rheology

In the study of the physical characteristics, through the development of the Strain sweep and the Frequency sweep analysis of our samples, we considered and obtained different coefficients, such as:

- The Storage modulus G': it represents the quantity of energy that is returnable in the form of elastic energy (elastic component), indicating how well the material can return to its original shape after deformation.
- The Loss modulus G": it represents the quantity of energy dissipated in the form of heat (plastic/viscoelastic component). It indicates how much energy is lost due to internal friction within the hydrogel.
- The tangent delta (tan δ): it is the ratio between Loss and Storage modulus (G"/G'). The higher, the more viscoelastic is the sample.
- The complex modulus G*: it is calculated as the square root of the sum of the squares of the Storage Modulus G' and Loss Modulus G". It provides an overall measure of the material's mechanical properties.

Here below are reported the graphs representing the various modules.

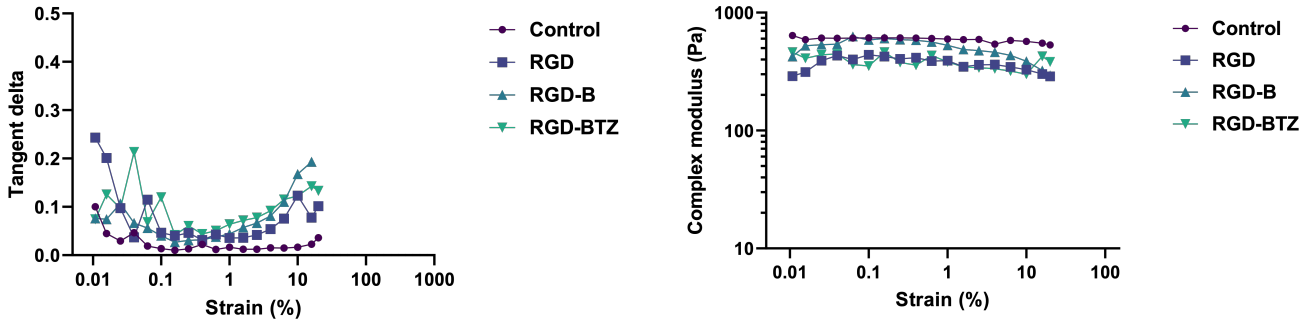

Figure 4.5: Graphics of the tangent delta and the complex modulus obtained with the Strain sweep analysis

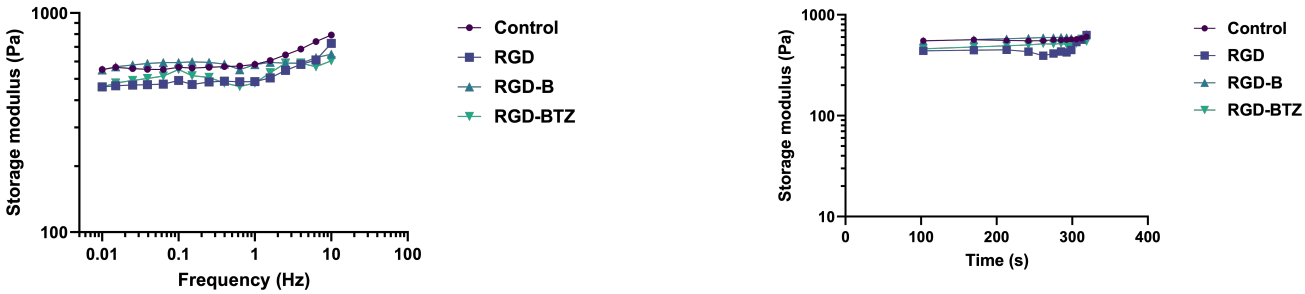

Figure 4.6: Graphics of the Storage modulus in function of frequency and time obtained with the Frequency sweep analysis

Figure 4.7: Graphics of the Loss modulus in function of frequency and time obtained with the Frequency sweep analysis

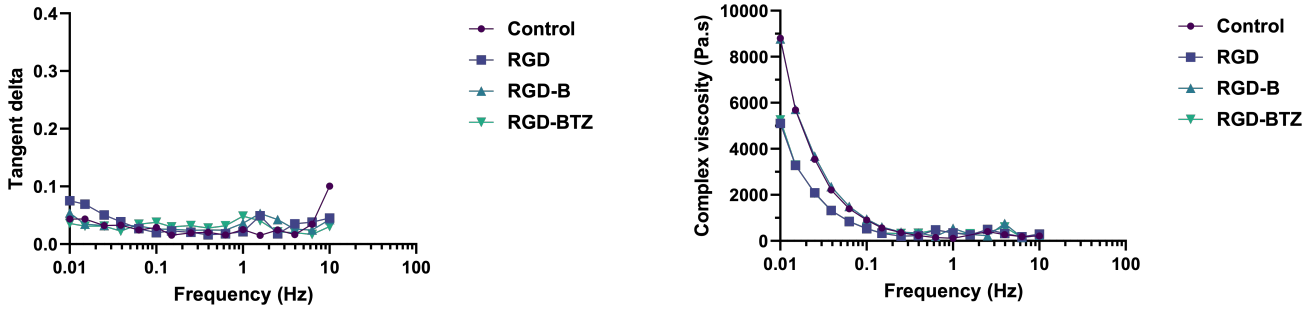

Figure 4.8: Graphics of the tangent delta and the complex viscosity obtained with the Frequency sweep analysis

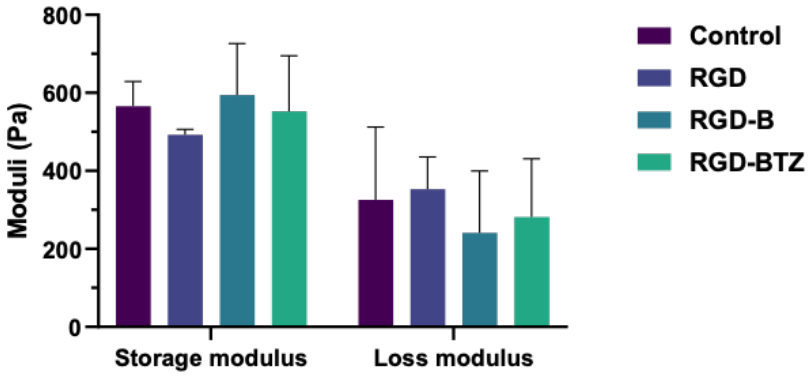

Figure 4.9: Storage and Loss modulus obtained from the tests of the different samples

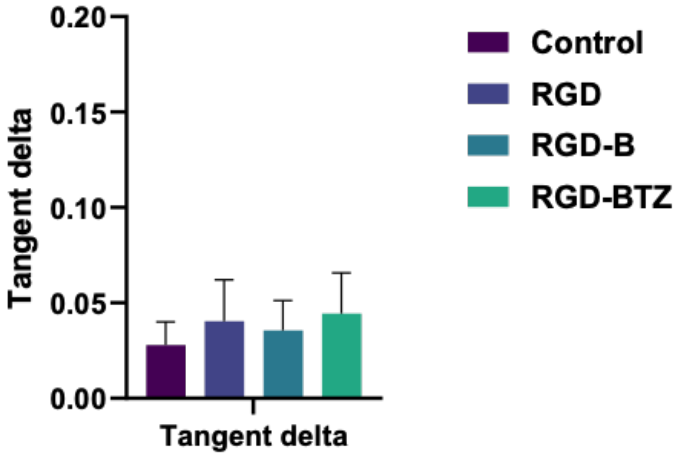

Figure 4.10: Tangent delta (tan δ) consequently calculated by the ratio of Loss and Storage modules

From the graphical data, we observed that the tangent delta (tan δ) of all the samples was very low. This finding confirms that our hydrogels exhibited predominantly elastic behavior. For this reason, a low tangent delta suggests that the hydrogels had a strong capacity to store and release elastic energy, returning to their original shape and form after deformation, with minimal energy loss as heat.
The predominance of the elastic component over the viscous component in our hydrogels is a desirable characteristic for many biomedical applications. For instance, in tissue engineering, an elastic hydrogel can provide a stable scaffold that supports cell growth and proliferation while maintaining its structural integrity under physiological conditions. Additionally, the consistency of these properties across all samples, irrespective of their specific conditions, highlights the robustness and reliability of our hydrogel formulation. This uniformity is crucial for ensuring predictable performance in clinical applications, where consistent mechanical properties are essential for safety and efficacy.

We calculated also the Young modulus for each condition, which, in general is a measure of the stiffness of a material when subjected to linear elastic deformation. It represents the ratio between the stress (tension) applied on a material, and the relative deformation (in this case the compression) that the material undergoes along the direction in which the force is applied (Hooke's law). In other words, Young's modulus measures the material's response to stress, during a static application, indicating how much the material stretches or compresses with respect to its original length when subjected to a force.

Here below is reported the formula (Equation 3) utilized for this calculus and obtained from the work of Dr. Anna Labernadie [113].

$$E = 2G'(1 + \nu)$$

Equation 3: Formula in which E is the Young modulus, G' is the Storage modulus and ν is the Poisson modulus which, for hydrogels, is 0.5

These are the results obtained calculating the Young modulus for each condition.

$$E_{CTRL} = 2G'_{CTRL}(1 + \nu) = 2\text{x}490(1 + 0.5) = 1650 \text{ Pa}$$

$$E_{RGD} = 2G'_{RGD}(1 + \nu) = 2\text{x}600(1 + 0.5) = 1470 \text{ Pa}$$

$$E_{RGD-B} = 2G'_{RGD-B}(1 + \nu) = 2\text{x}580(1 + 0.5) = 1800 \text{ Pa}$$

$$E_{RGD-BTZ} = 2G'_{RGD-BTZ}(1 + \nu) = 2\text{x}550(1 + 0.5) = 1740 \text{ Pa}$$

Equation 4: Results of the Young modulus for each condition (CTRLS, PEG-RGD, PEG-RGD-B and PEG-RGD-BTZ

Since the Young's modules seem to be rather low, our PEG hydrogels can easily deform under the application of moderate forces. This is consistent with the nature of hydrogels, which are designed to be flexible and to absorb large amounts of water.

4.3 In vitro assay

4.3.1 MTS assay

In this particular assay we proved the viability of our PEG hydrogels presenting boron compounds and the RGD sequence.
Here below are, in fact, reported the images of the two cell lines in the different conditions (dead control, live control, controls of PEG, PEG-RGD, PEG-RGD-Boron and PEG-RGD-Bortezomib) taken with the Nikon DS-Fi1 Microscope after the 24h and the 72h MTS assay. The cells seemed alive, healthy and in good conditions, confirming the biocompatibility of the material with human fibroblasts.

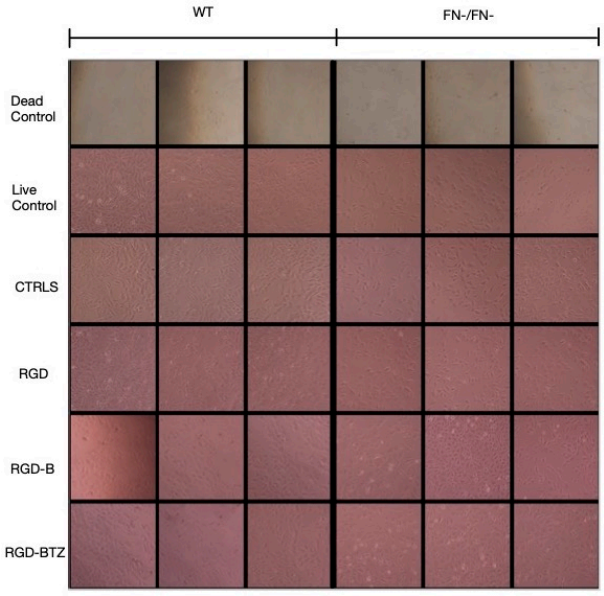

Figure 4.13: Cells photos of the 24h MTS assay

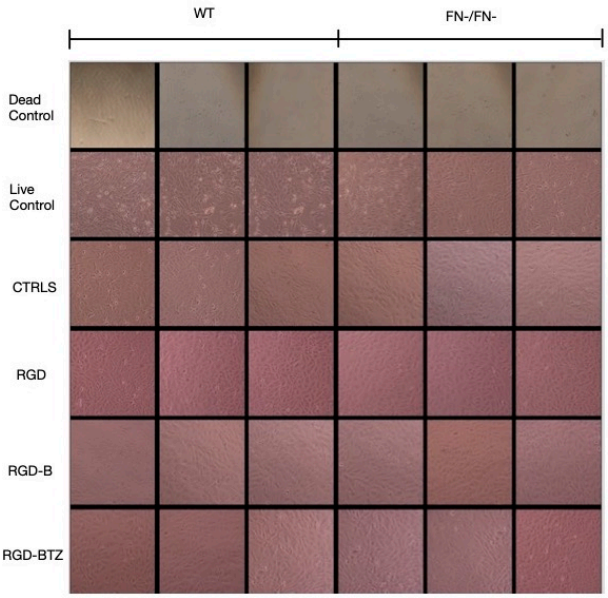

Figure 4.14: Cells photos of the 72h MTS assay

After the spectrophotometry, we obtained the data that were classified in the histograms below (Figures 4.15 and 4.16).
All the hydrogels seemed to present an almost zero citotoxicity, both at 24 hours and 72 hours, proving the stability of this quality over time. Both the cell lines in fact, the wild type (WT) and the mutated for the fibronectin (FN-/FN-), presented a high viability when put in contact with all the conditions of PEG hydrogels: controls of PEG, PEG-RGD, PEG-RGD-boron and PEG-RGD-Bortezomib.
In particular, it is pretty visible in the conditions with the RGD sequence and boron compounds how the viability of the cells seems even a bit higher than the others. This is probably due to the two main factors that favour the cellular adhesion (and so consequent cellular vitality): the RGD sequence and the boron compounds.
The RGD sequence, in fact, binds specifically to the binding sites of the integrins. The binding-integrins recognise and, once the RGD sequence binds to these integrins, a strong and specific bond is formed which promotes cell adhesion. This is a crucial step because it allows cells to remain stable and interact with their environment (when for example injected in a potential muscular site).
Simultaneously, the boron compounds activate the NaBC1 boron transporter.
The activated binding-integrins and the NABC1 together create a functional cluster which enhances the cellular proliferation too.

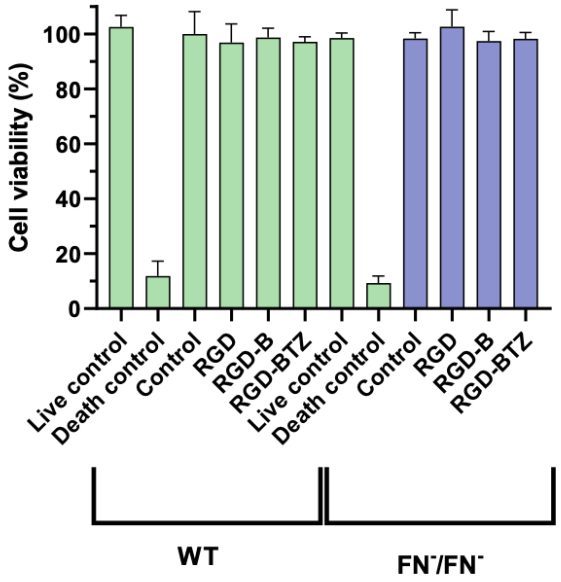

Figure 4.15: Results of the MTS assay at 24 hours

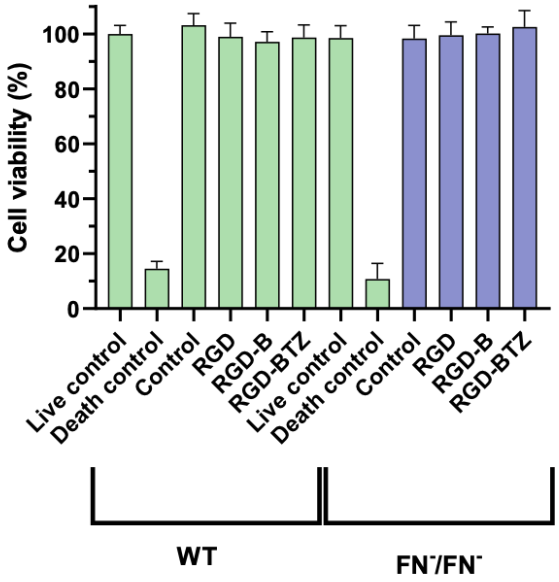

Figure 4.16: Results of the MTS assay at 72 hours

4.4 CAM assay

The Chorioallantoic membrane (CAM) serves as an essential extra embryonic membrane facilitating the exchange of nutrients and gases crucial for the embryo's sustenance during its developmental phase. Its important role extends beyond mere embryonic support: it has become a staple in vivo model for investigating angiogenic and anti-angiogenic responses elicited by various stimuli such as cells, tumors, or soluble factors [114]. Moreover, vascularization stands as a fundamental, multi-faceted process that is vital for various biological phenomena, including cell viability, embryonic maturation, tissue regeneration and reproductive function. Furthermore, it assumes a significant role in the progression of tumors, orchestrating their growth, infiltration and metastasis. Following injury, tissues undergo a shift towards hypoxia, depriving cells of the physiological blood supply essential for oxygenation, growth factors and cellular components crucial for natural repair mechanisms. In the realm of regenerative medicine, numerous attempts at tissue engineering have staggered due to the inability to stimulate adequate vascularization within constructs [115].

Consequently, there arises an urgent imperative to devise strategies that effectively promote the formation of functional vascular networks, thus ensuring the success of regenerative therapies. Despite its comparatively lower abundance in physiological contexts compared to ions like calcium or zinc, boron remains indispensable for cellular metabolism and holds promise as a catalyst for cell differentiation in vitro. The ion-channel NaBC1 emerges as a distinctive and precise boron transporter responsible for regulating intracellular boron levels [114].

For all these reasons, in this assay we expected to see an improvement of angiogenesis when introducing boron. In fact, as already explained before, a tissue that is functionally favourable and efficient must present a good vascularisation.
Here following are reported the photos taken of the blood vessels and the corresponding masks obtained with the ImageJ software, for each condition.

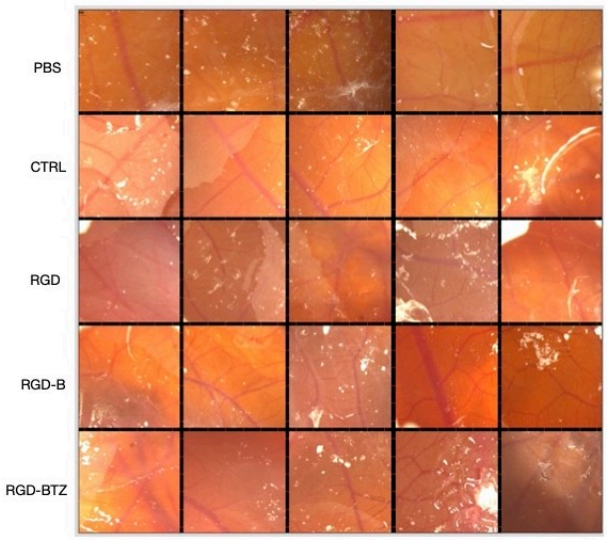

Figure 4.17: Photos taken of the Ferraravas-cularisation of the CAM for every condition

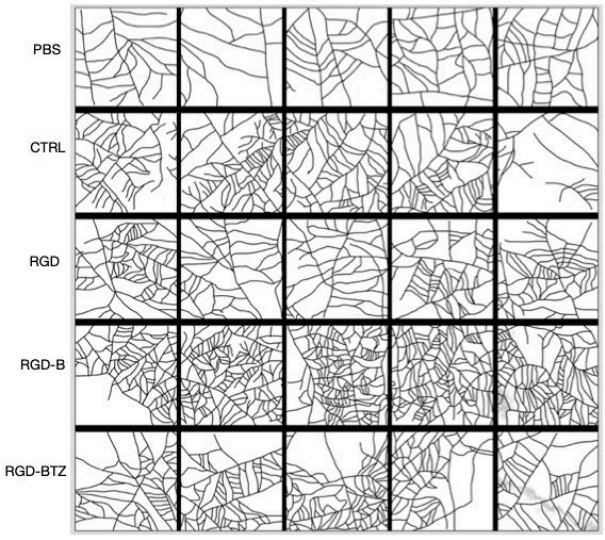

Figure 4.18: corresponding masks for the photos taken and reported on the left

The following graphs represent the results we obtained from our samples in the CAM assay. In particular, as explained previously, this particular analysis pointed out:

1. The lacunarity
2. The branching index
3. The number of end points
4. The number of junctions
5. The vessel density
6. The total vessel length
7. The average vessel length.

The meaning of these parameters was already deepened in Materials and Methods, in particular in the Table 3.1. (Summary of angiogenesis-related parameters analyzed with AngioTool software).

As it can be deduced from these graphs, the controls with just PEG hydrogels and the samples treated with PBS-/- exhibited similar levels of vascularization. This observation suggests that PEG, as a material, is inherently biocompatible and does not adversely affect angiogenesis. This is a crucial characteristic for materials intended for biomedical applications, as it indicates that PEG hydrogels can be utilized without disrupting the natural formation of blood vessels.
Moreover, the introduction of boron compounds significantly improved the structure of the blood vessels formation. Specifically, the samples of PEG-RGD-B (PEG hydrogels functionalized with both RGD sequences and boron) generated blood vessels with reduced lacunarity, indicating a more homogeneous and continuous vessel network.
These samples also showed a higher branching index, meaning there were more points where the vessels branched out, creating a more intricate and extensive vascular network. Additionally, there was an increase in the number of endpoints (the termini of vessel branches), the number of junctions (where vessels intersect), vessel density (the concentration of vessels within a given area), total vessel length and average vessel length compared to the other conditions tested.
The PEG-RGD-BTZ samples (PEG hydrogels with RGD sequences and Bortezomib) also demonstrated enhanced vascularization but to a slightly lesser extent than the PEG-RGD-Boron ones. This still confirms the efficacy of boron compounds in promoting angiogenesis more effectively than the RGD sequences alone. The addition of Bortezomib, an antineoplastic agent, seems to slightly moderate the angiogenic response, which might be attributed to its therapeutic effects on cell proliferation and survival.

In summary, these findings highlight the potential of PEG-RGD hydrogels with boron compounds in enhancing angiogenesis, making them promising candidates for applications in tissue engineering and regenerative medicine. By promoting the formation of a robust and well-structured vascular network, these hydrogels can significantly improve the integration and functionality of engineered tissues. The superior performance of boron-functionalized hydrogels underscores the importance of material modifications in optimizing biomedical materials for enhanced therapeutic outcomes.

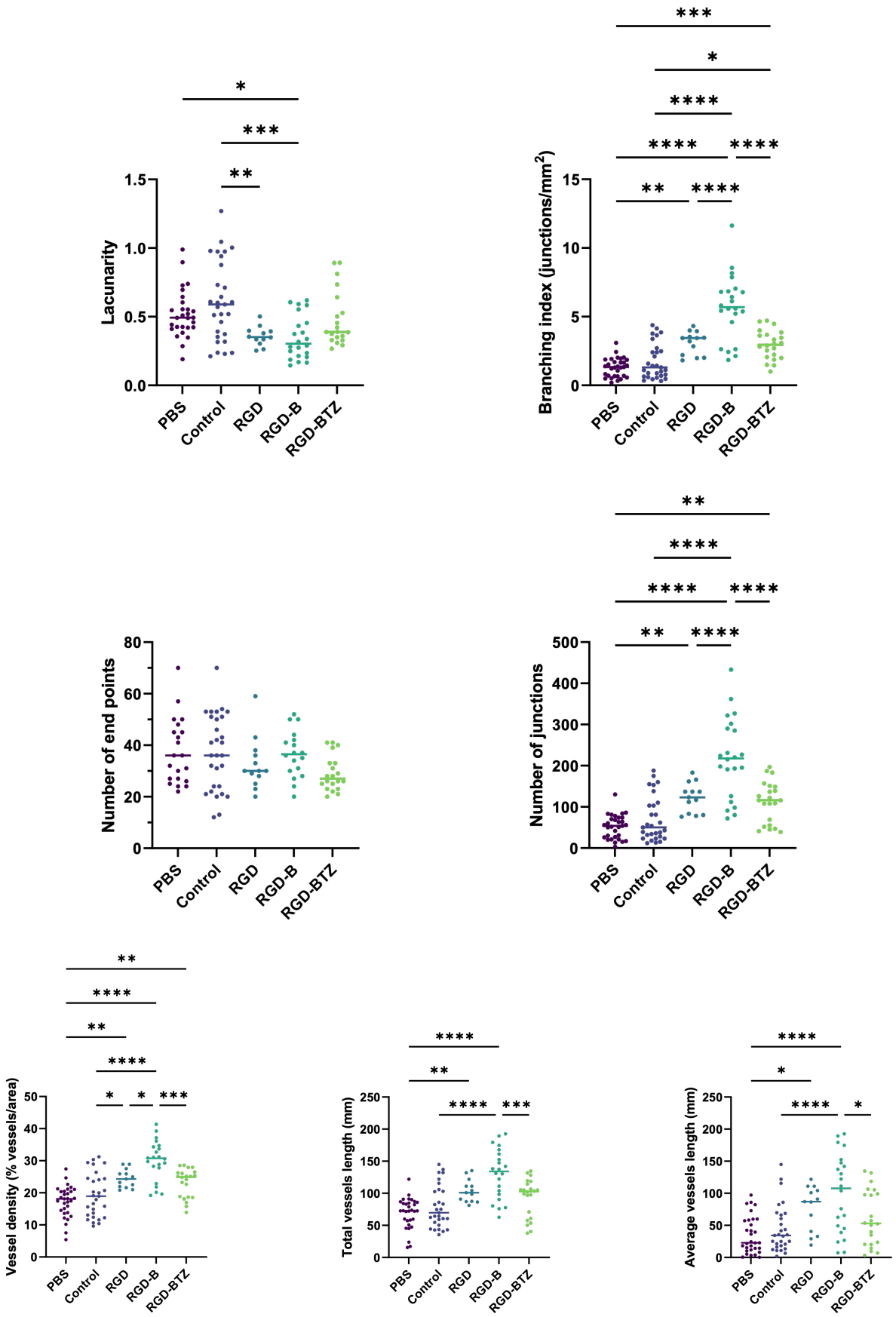

Figure 4.19: Representation of Lacunarity, Branching Index, Number of end points, Number of junctions, Vessels density, Total vessels length and Average vessels length obtained with Graph pad software, where the p value corresponds to: $* \leq 0.05; ** \leq 0.01; *** \leq 0.001; **** \leq 0.0001$.

Conclusions

Muscular injuries derived from trauma, ageing or pathological muscular conditions such as dystrophies, often necessitate invasive surgical interventions, transplants (autograft or allorgaft) or they don't even encounter a real solution (e.g. Duchenne or Becker dystrophies).
For these reasons, tissue engineering can represent a more efficient, resolutive and biocompatible answer.
In this master thesis project we developed PEG hydrogels composed of PEG-4MAL (polyethylene glycol with four terminal maleimide groups) and two crosslinkers at the same quantities (VPM and PEG-diSH). The VPM is degradable by metalloprotease MMPs while PEG-diSH is not. For this reason, utilized at the same quantities as we did, the crosslinkers determined a degradation rate of our material of the 50%.
These hydrogels were then enriched with: RGD (Arginine, Glycine and Aspartic Acid), a three-amminoacid adhesive sequence which can be found in fibronectin (a common protein present in the ECM) binded through PEGylation, and boron compounds such as Bortezomib, a drug utilized nowadays as inhibitor of the proteasome which consequently works as an anti-tumorigenic.
These two main components were introduced for the main reason to activate:
- through the boron, the NaBC1 boron transporter;
- through the RGD sequence, the binding-integrins present on the surface of the cells.
After the activation, the binding-integrins and the NaBC1 should create a functional cluster which would guarantee cellular adhesion, proliferation and differentiation.

In this master thesis work we mainly focused on the analysis of the material: its physico-chemical characteristics and its biocompatibility.
For the various tests we produced different samples, such as:
- CONTROLS: of just PEG
- PEG-RGD: PEG hydrogels with the RGD sequence
- PEG-RGD-B: PEG hydrogels with the RGD sequence and boron compounds
- PEG-RGD-BTZ: PEG hydrogels with the RGD sequence and Bortezomib

In particular, firstly it was conducted a Swelling assay. After submerging the hydrogels in MilliQ water for different time periods, we demonstrated their physical capability to absorb it, and, after a precise time period, their physical structure seemed to stabilize due to the crosslinkers.
In general, longer cross-linkers like PEG-diSH result in fact in hydrogels with higher swelling capacities, while shorter cross-linkers such as VPM limit expansion. All the conditions presented the same behaviour, highlighting the predictable and controllable nature of the hydrogels in this particular assay.

Afterwards, it was performed a Degradation assay. The samples were soaked in collagenase (a type of MMPs) for various time periods. The collagenase had the main purpose to degrade the bonds of the VPM determining the degeneration of the hydrogels consequently determining a mass loss. After the initial rapid phase of degradation, all the conditions reached a stabilization point around the 72-hour, which corresponds to the effective 50% degradation rate imposed for our PEG hydrogels.
This plateau signifies that half of the hydrogel matrix was degraded within this time-frame, primarily due to the enzymatic activity targeting the VPM sequences.
This consistent degradation pattern was observed across all conditions tested, indicating that the degradation process is reliable and reproducible.

Subsequently, the visco-elasticity of the material was testes. Through an hybrid rheometer, a strain sweep (with a constant frequency of 1Hz and a strain sweep between 0.01%-1%) and a frequency sweep (with an angular frequency between 0.01-10Hz and a constant strain of the 1%) were conducted.
In this analysis were calculated different modules: the Storage Modulus G', the Loss modulus G", the Tangent delta tan δ and the Young modulus.
The result gave a very low tangent delta (ratio between the plastic component and the elastic one) for all the samples. This demonstrated an elastic behaviour, certifying that the hydrogles had the capacity to return to their original shape and form after a deformation.

After the physico-chemical analysis of the material, it was tested its biocompatibility when in contact with human cells. In particular, an MTS assay was performed. This was based on the measurement of the absorbance through the spectrophotometer of the formazan (derived from the reduction of the MTS by the NADPH cells enzyme). We utilized two different cell lines of human fibroblasts: a wild-type (WT) and a mutant one (FN-/FN-) which didn't produce fibronectin.
In this assay, the material seemed to be highly compatible, with a zero toxicity rate, confirmed by the high viability of the cells after 24 and 72 hours. In particular, it is pretty visible in the conditions with the RGD sequence and boron compounds how the viability of the cells seems even a bit higher than the others. This is probably due to the

two main factors that favour the cellular adhesion (and so consequent cellular vitality): the RGD sequence and the boron compounds.

Finally, the hydrogels were tested in vivo too. We utilized twenty fertilized eggs we cut their shell and, without damaging their CAM (Chorioallantoid membrane), we positioned our hydrogels on top of their air chamber.
In this assay we produced five different conditions:
- PBS-/-: controls made of just the eggs with some PBS-/- on top of the CAM
- CONTROLS: eggs with PEG hydrogels
- PEG-RGD: eggs with PEG hydrogels enriched with the RGD sequence
- PEG-RGD-B: eggs with PEG hydrogels presenting the RGD sequence and boron compounds
- PEG-RGD-BTZ: eggs with PEG hydrogels enriched with RGD and Bortezomib
96 hours after implantation, incubating at 37°C, the sealings were removed and the vasculature was imaged using a stereomicroscope. With the analysis through the ImageJ and Angiotools software, we were able to highlight the main characteristics of the blood vessels, such as: the ramifications, the points and number of junctions (through the branching index), the lacunarity, the number of end points, the density and the total and average length.
The results demonstrated that controls with just PEG hydrogels and samples treated with PBS-/- showed similar vascularization levels, indicating that PEG is inherently biocompatible and does not adversely affect angiogenesis. Introducing boron compounds significantly enhanced blood vessel structure in PEG-RGD-B samples, resulting in a more homogeneous and extensive vascular network with increased branching, number of end points, junctions, vessel density and length. PEG-RGD-BTZ samples also improved vascularization, though slightly less than PEG-RGD-B, suggesting boron compounds promote angiogenesis more effectively than RGD alone, with Bortezomib potentially moderating the angiogenic response due to its effects on cell proliferation and survival.
The reason for this CAM assay was because a fundamental aspect for a functional and well reconstructed tissue is a good vascularisation, determined by a high number of vessels, junctions, and low lacunarity, which, consequently, guarantees the well-being of cells and the various transport mechanisms for their viability.

Looking at further future experiments, 2D (on top of the hydrogels) and 3D (sferoids inside of the hydrogels) in vitro analysis could be considered, utilizing for example immunofluorescence tecnique to verify focal adhesion domains.
Moreover, it could be evaluated also the option to utilize and conduct ulterior experiments with mutant cells that don't present binding-integrins, instead of just fibronectin.
Finally, a 100% degradation rate of the hydrogels could be imposed to verify the actual potential injection of these materials in a human body for the support of cell growth.

In conclusion, tissue engineering is becoming one of the most advanced experimental technologies for the biomedical sector, giving the possibility to the patient to regenerate the damaged area through its own cells, while introducing a degradable biomaterial that stimulates cell proliferation. In particular, the muscular regeneration could find many different field of application, giving the possibility to solve even pathologies that nowadays don't find any type of resolution.

Bibliography

[1] K. Mukund and S. Subramaniam, "Skeletal muscle: A review of molecular structure and function, in health and disease," *WIREs Syst Biol Med.; 12:e1462*, 2020.

[2] D. Exeter and D. Connell, "Skeletal muscle: Functional anatomy and pathophysiology," *emin Musculoskelet Radiol.*, 2010.

[3] R. Lieber and J. Fridén, "Clinical significance of skeletal muscle architecture," *Clin Orthop Relat Res.*, 2001.

[4] A. Martins, L. Giorno, and A. J. Santos, "Tissue engineering applied to skeletal muscle: Strategies and perspectives," *ioengineering (Basel). Nov 30;9(12):744.*, 2022.

[5] D. Manou, I. Caon, P. Bouris, *et al.*, "The complex interplay between extracellular matrix and cells in tissues," *Methods Mol Biol (Clifton, NJ)*, 2019.

[6] A. Theocharis, S. Skandalis, C Gialeli, and N. Karamanos, "Extracellular matrix structure," *Adv Drug Deliv Rev*, 2016.

[7] N. Karamanos, A. Theocharis, Z. Piperigkou, *et al.*, "A guide to the composition and functions of the extracellular matrix," *FEBS J, 288: 6850-6912*, 2021.

[8] C. Dalton and C. Lemmon, "Fibronectin: Molecular structure, fibrillar structure and mechanochemical signaling," *Cells.*, 2021.

[9] E. Ruoslahti, "Rgd and other recognition sequences for integrins," *Annu Rev Cell Dev Biol.;12:697-715.*, 1996.

[10] S. Akiyama, "Integrins in cell adhesion and signaling.," *Hum Cell.*, 1996.

[11] D. Erle and P. R., "How do integrins integrate? the role of cell adhesion receptors in differentiation and development," *Am J Respir Cell Mol Biol.*, 1992.

[12] J. Ciriza, A. Rodriguez-Romano, I. Nogueroles, *et al.*, "Borax-loaded injectable alginate hydrogels promote muscle regeneration in vivo after an injury," *Materials Science and Engineering C: Materials for Biological Applications (Online). (eissn: 1873-0191)*, 2021.

[13] R. Kreider, D. Kalman, J. Antonio, *et al.*, "International society of sports nutrition position stand: Safety and efficacy of creatine supplementation in exercise, sport, and medicine," *J Int Soc Sports Nutr. Jun 13;14:18.*, 2017.

[14] A. Shabbir, D. Zisa, L. M., C. Johnston, H. Lin, and T. Lee, "Muscular dystrophy therapy by nonautologous mesenchymal stem cells: Muscle regeneration without immunosuppression and inflammation," *Transplantation.*, 2009.

[15] M. Smoak and A. Mikos, "Advances in biomaterials for skeletal muscle engineering and obstacles still to overcome," *Mater. Today Bio.; 7100069.*, 2020.

[16] J. e. a. Grasman, "Biomimetic scaffolds for regeneration of volumetric muscle loss in skeletal muscle injuries," *Acta Biomater.; 25: 2-15*, 2015.

[17] A. Quintero, V. Wright, F. Fu, and J. Huard, "Stem cells for the treatment of skeletal muscle injury," *Clin. Sports Med. 28*, 2009.

[18] M. Lutolf and J. Hubbell, "Synthetic biomaterials as instructive extracellular microenvironments for morphogenesis in tissue engineering," *Nat. Biotechnol. 23, 47–55*, 2005.

[19] D. Kuraitis, C. Giordano, M. Ruel, A. Musaro', and E. Suuronen, *Biomaterials 33 428*, 2012.

[20] G. Mulbauer and H. Matthew, *Discoveries 7, e90*, 2019.

[21] P. Konieczny, S. Selma-Soriano, A. Rapisarda, and et al., *Drug Discov. Today 22 1740*, 2017.

[22] W. Liew and P. Kang, *Ther, Adv. Neurol. Dis. Ther. 6 147*, 2013.

[23] R. Chhabra, B. Ruozi, A. Vilella, and et al., *CNS Neurol. Disord. Drug Targets 14 1041*, 2015.

[24] H. Oliveira, S. Catros, C. Boiziau, and et al., *Acta Biomater. 29 435*, 2016.

[25] S. R. Caliari and J. A. Burdick, "A practical guide to hydrogels for cell culture," *Nat methods 13*, 2016.

[26] O. Alheib, L. da Silva, I. Kwon, R. Reis, and C. V.M., "Preclinical research studies for treating severe muscular injuries: Focus on tissue-engineered strategies," *Trends Biotechnol. May;41(5):632-652*, 2023.

[27] B. Alberts, D. Bray, J. Lewis, M. Raff, K. Roberts, and J. Watson, *Molecular biology of the cell*, 3rd ed. New York: Garland Publishing, Inc., 1994.

[28] O. Smidsr^d and S.-B. G., "Alginate as immobilization matrix for cells," *Trends Biotech;8:71–8.*, 1990.

[29] J. Suh and H. Matthew, "Application of chitosan-based polysaccharide biomaterials in cartilage tissue engineering: A review," *Biomaterials;21:2589–98*, 2000.

[30] C. Lee, A. Grodzinsky, and M. Spector, "The effects of cross-linking of collagen-glycosaminoglycan scaffolds on compressive stiff- ness, chondrocyte-mediated contraction, proliferation, and biosynthesis," *Biomaterials;22:3145–54*, 2001.

[31] C. Lee, A. Singla, and Y. Lee, "Biomedical applications of collagen," *Int J Pharm;221:1–22.*, 2001.

[32] S. Park, J. Park, H. Kim, M. Song, and H. Suh, "Characterization of porous collage/hyaluronic acid scaffold modified by 1- ethyl-3-(3-dimethylaminopropyl)carbodiimide cross-linking," *Biomaterials;23:1205–12*, 2002.

[33] W. Tan, R. Krishnaraj, and T. Desai, "Evaluation of nanostructured composite collagen–chitosan matricies for tissue engineering," *Tissue Eng;7:203–10*, 2001.

[34] G. Chen, T. Ushida, and T. Tateishi, "Development of biodegradable porous scaffolds for tissue engineering," *Mater Sci Eng C;17:63–9*, 2001.

[35] L. Huang, K. Nagapudi, R. Apkarian, and E. Chaikof, "Engineered collagen—peo nanofibers and fabrics," *J Biomater Sci: Polym Ed;12:979–93*, 2001.

[36] A. Theocharis, C Gialeli, V. Hascall, and N. Karamanos, "Extracellular matrix: A functional scaffold," *Walter de Gruyter GmbH Co KG, Berlin/Boston*, 2012.

[37] J. Fujiwara, M. Takahashi, T. Hatakeyama, and H. Hatakeyama, "Gelation of hyaluronic acid through annealing," *PolymInt;49:1604–8.*, 2000.

[38] G. Miralles, R. Baudoin, D. Dumas, *et al.*, "Sodium alginate sponges with or without sodium hyaluronate: In vitro engineering of cartilage," *J Biomed Mater Res;57: 268–78.*, 2001.

[39] F. Johnson, D. Craig, and A. Mercer, "Characterization of the block structure and molecular weight of sodium alginates," *J Pharm Pharmacol;49:639–43*, 1997.

[40] P. Eiselt, K. Lee, and M. D.J., "Rigidity of two-component hydrogels prepared from alginate and poly(ethylene glycol)- diamines," *Macromolecules;32:5561–6*, 1999.

[41] K. Lee, J. Rowley, P. Eiselt, E. Moy, K. Bouhadir, and D. Mooney, "Controlling mechanical and swelling properties of alginate hydrogels independently by cross-linker type and cross-linking density," *Macromolecules;33:4291–4*, 2000.

[42] M. LeRoux, F. Guilak, and L. Setton, "Compressive and shear properties of alginate gel: Effects of sodium ions and alginate concentration," *J Biomed Mater Res;47:46–53*, 1999.

[43] K. Lee, K. Bouhadir, and D. Mooney, "Degradation behavior of covalently cross-linked poly(aldehyde guluronate) hydrogels," *Macromolecules;33:97–101*, 2000.

[44] Y. Zhang and M. Zhang, "Synthesis and characterization of macro- porous chitosan/calcium phosphate composite scaffolds for tissue engineering," *J Biomed Mater Res;55:304–12*, 2001.

[45] A. Chenite, C. Chaput, D. Wang, *et al.*, "Novel injectable neutral solutions of chitosan form biodegradable gels in situ," *Biomaterials;21:2155–61*, 2000.

[46] J. Drury and D. Mooney, "Hydrogels for tissue engineering: Scaffold design variables and applications," *Biomaterials 24 4337–4351*, 2003.

[47] T Al Kayal, P Losi, S Pierozzi, and G. Soldani, "New method for fibrin-based electrospun/sprayed scaffold fabrication," *Sci Rep. Mar 20*, 2020.

[48] M. Tibbitt and K. Anseth, "Hydrogels as extracellular matrix mimics for 3d cell culture," *Biotechnol. Bioeng. 103, 655–663*, 2009.

[49] T. Khan, K. Peh, and H. Ch'ng, "Mechanical, bioadhesive strength and biological evaluations of chitosan films for wound dressing," *J Pharm Pharmaceut Sci.; 3:303–311*, 2000.

[50] A. Mahdavi, "A biodegradable and biocompatible gecko-inspired tissue adhesive," *Proc Natl Acad Sci USA*, 2008.

[51] J. Di, "Stretch-triggered drug delivery from wearable elastomer films containing therapeutic depots," *ACS Nano.; 9:9407–9415*, 2015.

[52] J. Li and D. Mooney, "Designing hydrogels for controlled drug delivery," *Nat Rev Mater*, 2016.

[53] L. Suggs and A. Mikos, "Development of poly(propylene fumarate- co-ethylene glycol) as an injectable carrier for endothelial cells," *Cell Trans;8:345–50*, 1999.

[54] A. D'souza and R. Shegokar, "Polyethylene glycol (peg): A versatile polymer for pharmaceutical applications," *Expert Opin Drug Deliv.*, 2016.

[55] S Essa, J. Rabanel, and P Hildgen, "Effect of polyethylene glycol (peg) chain organization on the physicochemical properties of poly(d, l-lactide) (pla) based nanoparticles.," *Eur J Pharm Biopharm.*, 2010.

[56] N. A. Peppas, P. Bures, W. Leobandung, and H. Ichikawa, "Hydrogels in pharmaceutical formulations," *Eur. J. Pharm. Biopharm. 50:27–46*, 2000.

[57] N. Peppas, K. B. Keys, M. Torres-Lugo, and A. M. Lowman, "Poly(ethylene glycol)-containing hydrogels in drug delivery," *J. Control. Release. 62:81–87*, 1999.

[58] S. J. Bryant, C. R. Nuttelman, and K. S. Anseth, "Cytocompatibility of uv and visible light photoinitiating systems on cultured nih/3t3 fibroblasts in vitro," *J. Biomater. Sci. Polym. Ed. 11:439–457*, 2000.

[59] J. A. Burdick and K. S. Anseth, "Photoencapsulation of osteoblasts in injectable rgd-modified peg hydrogels for bone tissue engineering," *Biomaterials. 23:4315–4323*, 2002.

[60] C. Lin and K. Anseth, "PEG hydrogels for the controlled release of biomolecules in regenerative medicine," *Pharmaceutical Research, Vol. 26, No. 3*, 2009.

[61] G. Csucs, R. Michel, J. W. Lussi, M. Textor, and G. Danuser, "Microcontact printing of novel co-polymers in combination with proteins for cell-biological applications," *Biomaterials. 24:1713– 1720*, 2003.

[62] L. M. Weber, K. N. Hayda, K. Haskins, and K. S. Anseth, "The effects of cell-matrix interactions on encapsulated beta-cell function within hydrogels functionalized with matrix-derived adhesive peptides," *T. Biomaterials. 28:3004–3011*, 2007.

[63] K. Antonsen and A. Hoffman, "Water structure of peg solutions by differential scanning calorimetry measurements," *J.M Harris (Ed.), Poly(ethylene glycol) Chemistry: Biotechnical and Biomedical Applications, Plenum Press, New York*, 1992.

[64] N. A. Peppas, K. B. Keys, M. Torres-Lugo, and A. M. Lowman, "Poly(ethylene glycol)-containing hydrogels in drug delivery," *J. Control. Release. 62:81–87*, 1999.

[65] K. Wolf, R. Muller, S. Borgmann, E. B. Brocker, and P. Friedl, "Amoeboid shape change and contact guidance: T-lymphocyte crawling through fibrillar collagen is independent of matrix remodeling by mmps and other proteases," *Blood. 102:3262–3269*, 2003.

[66] K. Wolf, I. Mazo, H. Leung, *et al.*, "Compensation mechanism in tumor cell migration: Mesenchymal-amoeboid transition after blocking of pericellular proteolysis," *J. Cell Biol. 160: 267–277*, 2003.

[67] P. Friedl, F. Entschladen, C. Conrad, B. Niggemann, and K. S. Zaenker, "T lymphocytes migrating in 3-d collagen lattices lack focal adhesions and utilize b1 integrin-independent strategies for polarization, interaction with collagen fibres, and migration," *Eur. J. Immunol. 28:2331–2343*, 1998.

[68] S. L. Schor, T. D. Allen, and B. Winn, "Lymphocyte migration into three-dimensional collagen matrices: A quantitative study," *J. Cell Biol. 96:1089–1096*, 1983.

[69] Y. Hegerfeldt, M. Tusch, E. B. Brocker, and P. Friedl, "Collective cell movement in primary melanoma explants: Plasticity of cell-cell interaction, beta1-integrin function, and migration strategies," *C. Cancer Res. 62:2125–2130*, 2002.

[70] G. Raeber, M. Lutolf, and J. Hubbell, "Molecularly engineered PEG hydrogels: A novel model system for proteolytically mediated cell migration," *Biophysical Journal, Volume 89*, 2005.

[71] R. Shi, R. Borgens, and A. Blight, "Functional reconnection of severed mammalian spinal cord axons with polyethylene glycol," *Journal of neurotrauma Volume 16, Number 8, Mary Ann Liebert, Inc.*, 1999.

[72] J. Burdick and K. Anseth, "Photoencapsulation of osteoblasts in injectable RGD-modified PEG hydrogels for bone tissue engineering," *Biomaterials 23 4315–4323*, 2002.

[73] A. Edward, N. Landázuric, P. Thuléd, W. R. Taylorc, and A. Garcíaa, "Bioartificial matrices for therapeutic vascularization," *Applied biological sciences*, 2009.

[74] P. Yurchenco, *Cold Spring Harb. Perspect. Biol. 3, a004911*, 2011.

[75] Y. Wang, N. Dumont, and M. Rudnicki, *J. Cell Sci. 127 4543*, 2014.

[76] L. Lukjanenko, M. Jung, N. Hegde, *et al.*, *Nat. Med. 22 897*, 2016.

[77] B. Hille, "Ion channels of excitable membranes," *Sinauer Associates, Oxford*, 2001.

[78] I. Lauritzen, J. Chemin, E. Honor e, *et al.*, *EMBO Rep. 6 642*, 2005.

[79] A. Gasparski and K. Beningo, *Arch. Biochem. Biophys. 586 20*, 2015.

[80] A. Schwab, A. Fabian, P. Hanley, and C. Stock, *Physiol. Rev. 92 1865.*, 2012.

[81] A. Becchetti and A. Arcangeli, *Adv. Exp. Med. Biol 674 107*, 2010.

[82] M. Park, Q. Li, N. Shcheynikov, W. Zeng, and S. Muallem, *Mol. Cell 16 331*, 2004.

[83] P. Rico, A. Rodrigo-Navarro, M. de la Peña, V. Moulisov'a, M. Costell, and M. Salmeron-Sanchez, *Adv. Biosyst. 3, 1800220*, 2018.

[84] H. Apdik, A. Dogan, S. Demirci, S. Aydin, and F. Sahin, *Biol. Trace Elem. Res. 165 123*, 2015.

[85] W. Yang, X. Gao, and B. Wang, *Med. Res. Rev. 23 346*, 2003.

[86] S. Danti, G. Ciofani, G. Pertici, *et al.*, *Tissue Eng. Regen. Med. 9 847*, 2015.

[87] P. Balasubramanian, T. Bütner, V. Miguez Pacheco, and A. Boccaccini, *J. Eur. Ceram. Soc. 38 855*, 2018.

[88] F. Nielsen, "Evidence for the nutritional essentiality of boron," *J Trace Elem Exp Med 9, 215,*, 1996.

[89] F. Nielsen and J. Penland, "Boron supplementation of peri-menopausal women affects boron metabolism and indices associated with macromineral metabolism, hormonal status and immune function," *J Trace Elem Exp Med 12, 215*, 1999.

[90] R. Kane, P. Bross, A. Farrell, Pazdur, and R. Velcade, "U.s. fda approval for the treatment of multiple myeloma progressing on prior therapy," *Oncologist 8, 508*, 2003.

[91] W. Yang, X. Gao, and B. Wang, "Boronic acid compounds as potential pharmaceutical agents," *Med Res Rev 23, 346*, 2003.

[92] R. Brown, M. Rahaman, A. Dwilewicz, *et al.*, "Effect of borate glass composition on its conversion to hydroxyapatite and on the proliferation of mc3t3-e1 cells," *J Biomed Mater Res A 88, 392*, 2009.

[93] C. Wu, R. Miron, A. Sculean, *et al.*, "Proliferation, differentiation and gene expression of osteoblasts in boron-containing associated with dexamethasone deliver from mesoporous bioactive glass scaffolds," *Biomaterials 32, 7068*, 2011.

[94] M. Rahaman, D. Day, B. Bal, *et al.*, "Bioactive glass in tissue engineering," *Acta Biomater 7, 2355*, 2011.

[95] J. Gough, P. Christian, C. Scotchford, and I. Jones, "Craniofacial osteoblast responses to polycaprolactone produced using a novel boron polymerisation technique and potassium fluoride post-treatment," *Biomaterials 24, 4905*, 2003.

[96] H. Apdik, A. Dog an, S. Demirci, S. Aydın, and F. Sxahin, "Dose-dependent effect of boric acid on myogenic differ- entiation of human adipose-derived stem cells (hadscs)," *Biol Trace Elem Res 165, 123*, 2015.

[97] C. Dordas, M. Chrispeels, and P. Brown, "Permeability and channel-mediated transport of boric acid across membrane vesicles isolated from squash roots," *Plant Physiol 124, 1349*, 2000.

[98] P. Rico, A. Rodrigo-Navarro, and M. Salmerón-Sánchez, "Borax-loaded plla for promotion of myogenic differentiation," *Tissue Eng Part A.;21(21-22):2662-72.*, 2015.

[99] K. Tanaka, K. Sato, T. Yoshida, *et al.*, "Evidence for cell density affecting c2c12 myogenesis: Possible regulation of myogenesis by cell-cell communication," *Muscle Nerve 44, 968*, 2011.

[100] P. Carmeliet, *Nature 438, 932.* 2005.

[101] V. Moulisová, C. Gonzalez-García, M. Cantini, *et al.*, "Biomaterials, 126, 61," 2017.

[102] P. Briquez, L. Clegg, M. Martino, F. Gabhann, and J. Hubbell, "Nat. rev. mater., 1, 15006," 2016.

[103] P. Carmeliet and R. Jain, "Nature, 473, 298," 2011.

[104] R. Hynes, "Cell, 110, 673," 2002.

[105] G. Mahabeleshwar, W. Feng, K. Reddy, E. Plow, and T. Byzova, "Circ. res., 101, 570," 2007.

[106] A. Olsson, A. Dimberg, J. Kreuger, and L. Claesson-Welsh, "Nat. rev. mol. cell biol., 7, 359," 2006.

[107] R. Alexander, G. W. Prager, J. Mihaly-Bison, *et al.*, "Cardiovasc. res., 94, 125," 2012.

[108] S. Herkenne, C. Paques, O. Nivelles, *et al.*, "Sci. signaling, 8, 1," 2015.

[109] I. Lauritzen, J. Chemin, E. Honoré, *et al.*, "Embo rep., 6, 642," 2005.

[110] A. N. Gasparski and K. A. Beningo, "Arch. biochem. biophys., 586, 20," 2015.

[111] L. Munaron, T. Genova, D. Avanzato, S. Antoniotti, and A. Fiorio, "Pla, recent pat. anti-cancer drug discovery., 8, 27," 2013.

[112] O.-C. L., M.-G. H., G.-G. C., S.-S. M., G. MP., and M.-M. C., "Protease-degradable hydrogels with multifunctional biomimetic peptides for bone tissue engineering," *Front Bioeng Biotechnol. 1;11:1192436.*, 2023 Jun.

[113] A. Labernadie, A. Bouissoul, P. Delobelle, *et al.*, "Protrusion force microscopy reveals oscillatory force generation and mechanosensing activity of human macrophage podosomes," *Nature communications*, 11 Nov 2014.

[114] P. Rico, A. Rodrigo-Navarro, M. de la Peña, and M. Salmerón-Sánchez, "Simultaneous boron ion-channel/growth factor receptor activation for enhanced vascularization," *Advanced Biosystems 3(1):1800220*, October 2018.

[115] D. Ribatti, "Chick embryo chorioallantoic membrane as a useful tool to study angiogenesis," *Int Rev Cell Mol Biol.*, 2008.